JUN 10 1959 DECLASSIFIED

NASA MEMO 6-9-59L

CLASSIFICATION CANCELLED
AUTHORITY NASA TECHNICAL PUBLICATIONS
ANNOUNCEMENTS NO. _____ DATE _____ BY _____

CASE FILE COPY

NASA

MEMORANDUM

N-02
P52 39456

WIND-TUNNEL MEASUREMENTS OF EFFECT OF DIVE-RECOVERY FLAPS AT TRANSONIC SPEEDS ON MODELS OF A SEAPLANE AND A TRANSPORT

By Atwood R. Heath, Jr., and Robert J. Ward

Langley Research Center
Langley Field, Va.

NASA FILE COPY
loan expires on last
date stamped on back cover.
PLEASE RETURN TO
DIVISION OF RESEARCH INFORMATION
NATIONAL AERONAUTICS
AND SPACE ADMINISTRATION
Washington 25, D. C.

CLASSIFIED DOCUMENT - TITLE UNCLASSIFIED

This material contains information affecting the National Defense of the United States within the meaning of the espionage laws, Title 18, U.S.C., Secs. 793 and 794, the transmission or revelation of which in any manner to an unauthorized person is prohibited by law.

NATIONAL AERONAUTICS AND SPACE ADMINISTRATION

WASHINGTON

June 1959

DECLASSIFIED

NATIONAL AERONAUTICS AND SPACE ADMINISTRATION

MEMORANDUM 6-9-59L

WIND-TUNNEL MEASUREMENTS OF EFFECT OF DIVE-RECOVERY FLAPS AT TRANSONIC SPEEDS ON MODELS OF A SEAPLANE AND A TRANSPORT*

By Atwood R. Heath, Jr., and Robert J. Ward

SUMMARY

The effects of wing-lower-surface dive-recovery flaps on the aerodynamic characteristics of a transonic seaplane model and a transonic transport model having 40° swept wings have been investigated in the Langley 16-foot transonic tunnel. The seaplane model had a wing with an aspect ratio of 5.26, a taper ratio of 0.333, and NACA 63A series airfoil sections streamwise. The transport model had a wing with an aspect ratio of 8, a taper ratio of 0.3, and NACA 65A series airfoil sections perpendicular to the quarter-chord line. The effects of flap deflection, flap longitudinal location, and flap sweep were generally investigated for both horizontal-tail-on and horizontal-tail-off configurations. Model force and moment measurements were made for model angles of attack from -5° to 14° in the Mach number range from 0.70 to 1.075 at Reynolds numbers of 2.95×10^6 to 4.35×10^6.

With proper longitudinal location, wing-lower-surface dive-recovery flaps produced lift and pitching-moment increments that increased with flap deflection. For the transport model a flap located aft on the wing proved to be more effective than one located more forward, both flaps having the same span and approximately the same deflection. For the seaplane model a high horizontal tail provided added effectiveness for the deflected-flap configuration.

INTRODUCTION

The possibility that transports and bombers designed for high-subsonic and transonic speeds may encounter adverse compressibility effects has revived interest in auxiliary control devices. These

*Title, Unclassified.

adverse compressibility effects become evident in the form of trim changes due to increased longitudinal stability and high control forces due to excess hinge moments. A wing-mounted dive-recovery flap has in the past been found capable of producing the large changes in lift and pitching moment needed to assist the pilot in pulling out of high-subsonic-speed dives (ref. 1).

The problems associated with the longitudinal stability first appeared during World War II when fighter airplanes encountered compressibility effects in high-speed dives. The use of dive-recovery flaps on these airplanes proved to be the solution. (See refs. 2 and 3.) Transonic bombers and transports differ from these fighters in that the former have swept wings while the latter all had straight wings. However, all the airplanes are similar in one respect - they all have relatively thick wing sections which are highly susceptible to compressibility effects. The possibility exists, therefore, that inadvertent overspeeding in level flight because of excess engine power could result in large negative pitching moments and excessive tail loads. Under such circumstances dive-recovery flaps may provide a means for alleviating these conditions. Little is known about the effects of flap location, flap deflection, Mach number, and horizontal-tail location on the action of dive-recovery flaps. However, some information is available in reference 4 on flap longitudinal location on a 15-percent-thick airfoil.

The present investigation was exploratory in nature in order to obtain results on the effects of wing-lower-surface dive-recovery flaps installed on a seaplane model and on a transport model. The investigation was conducted in the Langley 16-foot transonic tunnel over a Mach number range from 0.70 to 1.075 and an angle-of-attack range from -5° to 14°. Force and moment data are presented for both tail-on and tail-off configurations. The Reynolds number based on the wing mean aerodynamic chord varied from 2.95×10^6 to 4.35×10^6.

SYMBOLS

b	wing span
C_D	drag coefficient, Drag/qS
C_L	lift coefficient, Lift/qS
C_m	pitching-moment coefficient about quarter chord of wing mean aerodynamic chord, Pitching moment/qSc'

ΔC_L change in lift coefficient due to flap deflection (at constant angle of attack)

ΔC_m change in pitching-moment coefficient due to flap deflection

c local wing chord measured parallel to body reference line or waterline

c' wing mean aerodynamic chord

c_r wing root chord

M Mach number

q free-stream dynamic pressure

S wing area (includes area covered by body)

t wing-section maximum thickness

y spanwise distance measured from the body plane of symmetry

α angle of attack of body reference line or waterline

α_w angle of attack of wing root chord

Subscripts:

D indicates change in tail loading due to wing downwash

i indicates constant angle of attack

w wing contribution (tail off)

t indicates constant lift coefficient

$\Delta\alpha$ indicates change in angle of attack

MODELS AND APPARATUS

Models

Transonic seaplane model.- A two-view sketch of the seaplane model is shown in figure 1(a) and a photograph of the model installed in the Langley 16-foot transonic tunnel is shown in figure 1(b).

[redacted]

The wing which was made of steel had an aspect ratio of 5.26, a taper ratio of 0.333, and a sweepback of the quarter-chord line of 40°. The airfoil sections in a streamwise direction were the NACA 63A series with 0.3 camber. The thickness ratio varied from 0.11 at the root to 0.08 at the tip; the wing-section incidence, relative to the waterline, varied from 3.0° at the root to -2.0° at the tip. Figure 2 gives the spanwise variation of thickness ratio and wing geometric twist.

The horizontal tail had an aspect ratio of 3.5, a taper ratio of 0.4714, sweepback of the quarter chord of 40°, and NACA 63A009 airfoil sections. The horizontal tail was located at the top of the vertical tail and the tail root chord was located 0.308 wing semispan above a line through the wing leading-edge apex parallel to the waterline.

Transonic transport model.- A two-view sketch of the model is shown in figure 3(a) and a photograph of the model installed in the Langley 16-foot transonic tunnel is shown in figure 3(b).

The wing, which was made of steel, had an aspect ratio of 8.0, a taper ratio of 0.3, and a sweepback of the quarter-chord line of 40°. The airfoil sections perpendicular to the quarter-chord line were the NACA 65A series cambered for a wing lift coefficient of 0.514 with an approximately elliptical span loading. The thickness ratio streamwise varied from 0.12 at the root to 0.06 at the tip and the wing-section incidence streamwise varied from 5.65° at the 0.05 semispan station to -2.90° at the tip. Figure 2 gives the spanwise variation of thickness ratio and wing geometric twist.

The horizontal tail had an aspect ratio of 4.0, a taper ratio of 0.3, sweepback of the quarter-chord line of 40°, and NACA 65A006 airfoil sections streamwise. The tail was located on the body 0.031 wing semispan below a plane through the wing leading edge parallel to the fuselage center line which was alined with the free-stream airflow at 0° angle of attack. No vertical tail was used for this investigation.

The shape of the transport body in the region of the wing was obtained by superposition of the streamline contours, at design lift coefficient, on an area distribution for the $M = 1.0$ area rule.

Dive-recovery flaps.- The flaps were made of wood and were glued to the lower surface of the wing. The flaps have been considered to be wing-mounted flaps, whereas in actual practice they might be mounted on the body which could be advantageous from a structural standpoint.

Three flap configurations were tested on the seaplane and sketches of these flaps are shown in figure 4(a). In two configurations, the flaps were located 0.07 inch behind the 0.65-chord line and both flaps

[redacted]

extended from the body to 0.35 semispan. One flap was deflected 30° about the hinge line while the second flap was deflected 45°. The third configuration consisted of an unswept flap located at 0.84 root chord. The flap extended from the body to the 0.267-semispan station and was deflected 30° about the hinge line.

Four flap configurations were tested on the transport model and sketches of these flaps are shown in figure 4(b). The first configuration consisted of a swept flap deflected 35.5°, located at the 0.65 chord line, and extended from the body to 0.25 semispan. The second configuration consisted of a swept flap deflected 36.8°, located at the 0.30 chord line, and extended from the body to 0.25 semispan. The last two configurations consisted of unswept flaps deflected 90° with each flap extending from the body to 0.15 semispan. One flap was located at 0.80 root chord and the other was located at 0.50 root chord.

Photographs of typical flap installations on both models are shown in figure 5.

Apparatus

The investigation was conducted in the Langley 16-foot transonic tunnel which is a single-return octagonal slotted-throat wind tunnel. A detailed description of the tunnel is given in reference 5. The models were supported by a sting attached to the support strut which changed angle of attack in such a way that the models were kept close to the tunnel center line.

The model forces and moments were measured by an internal three-component strain-gage balance. Two different balances were used, one for the seaplane model and another for the transport model. The model angles of attack were measured for each test point by means of a pendulum-type strain-gage inclinometer located inside the model.

TESTS

Transonic Seaplane Model

Tests on the seaplane model were conducted over a Mach number range from 0.80 to 1.075 and over a wing-root-chord angle-of-attack range from -4° to 14°. The Reynolds number, based on the wing mean aerodynamic chord, varied from 2.95×10^6 to 3.76×10^6. Four model configurations were tested with the horizontal tail off. The first configuration consisted of the basic model with no dive-recovery flaps.

The three remaining configurations tested had dive-recovery flaps as shown in figure 4(a). With the exception of the model with the unswept 0.84-root-chord flap deflected 30°, all other configurations were then tested with the horizontal tail added to the model. The tail incidence was set at 0° to the waterline which is -3° to the wing root chord. Transition was fixed on the wing by means of a 1/8-inch-wide strip of abrasive particles located at 10 percent of the local wing chord.

Transonic Transport Model

Tests on the transport model were made over a Mach number range from 0.70 to 0.92 and over an angle-of-attack range from -5° to 4°. The Reynolds number, based on wing mean aerodynamic chord, varied from 3.50×10^6 to 4.35×10^6. The model was tested in five configurations with the horizontal tail off. The first configuration consisted of the basic model with no dive-recovery flaps. The four remaining configurations tested were the configurations with dive-recovery flaps shown in figure 4(b). With the exception of the model with the unswept 0.50-root-chord flap deflected 90°, all other configurations were then tested with the horizontal tail added to the model at a tail incidence of -1° to the body reference line. Transition was fixed on the wing by means of a 1/8-inch-wide strip of abrasive particles located at $2\frac{1}{2}$ percent of the local wing chord.

CORRECTIONS AND ACCURACY

The model angles of attack have been corrected for a tunnel upwash angle of 0.17° which was determined from previous tests in the 16-foot transonic tunnel. Based on instrument accuracy and repeatability of data, the model angles of attack are believed to be accurate to ±0.1°.

The chord-force component of the balance failed part way through the tests of the seaplane model so that no drag coefficients are available for several configurations. Estimated values of chord force obtained from previous tests of the model were used in the transferral of pitching moments from the balance center to the quarter chord of the wing mean aerodynamic chord. The estimated values of chord force were also used in determining lift coefficients, where required. The drag data presented have not been corrected for the internal drag of the nacelles on the seaplane model. All force data have been adjusted to the condition of free-stream static pressure at the model base.

The following table shows the accuracy of the aerodynamic coefficients based on instrument error at a Mach number of 0.80:

	Seaplane model	Transport model
C_L	±0.0070	±0.0070
C_D	±.0015	±.0006
C_m	±.0020	±.0015
ΔC_L	±.0140	±.0140
ΔC_m	±.0040	±.0030

No corrections have been made for either wing aeroelasticity or sting interference.

RESULTS AND DISCUSSION

The aerodynamic characteristics of the basic models and of the various flap configurations for both the seaplane and the transport are presented in figures 6 to 12. For the following discussion of the basic data, the flap effectiveness is considered to be the change in pitching-moment coefficient, due to flap deflection, at constant lift coefficient.

Transonic Seaplane Model

Figures 6 and 7 show the effect of deflected flaps on the aerodynamic characteristics of the model for the tail-on condition. Flap deflection causes an increase in lift coefficient at all Mach numbers and at angles of attack from -4° to at least 4°, and in many cases up to 10° or 12°. As would be expected, the larger flap deflection gives the larger increase in lift. The deflected flaps generally caused an increase in pitching-moment coefficient at all Mach numbers. A comparison of the swept-flap data of figure 6 and the unswept-flap data of figure 7 shows that, for the same flap deflection (30°) the unswept flap of small span was as effective in producing a positive increment in pitching moment as the swept flap of greater span. For all Mach numbers, a sizable increase in drag is noted for all flap deflections. Although the main intent in the use of dive-recovery flaps is to obtain increases in lift and pitching moment, the increase in drag might result, in some

cases, in slowing down the airplane enough to alleviate the longitudinal stability difficulties.

Figure 8 shows the effect of deflected swept flaps on the aerodynamic characteristics of the basic seaplane model for the horizontal-tail-off condition. Increases in lift coefficients for the deflected-flap configurations are of roughly the same order as were observed for the tail-on configurations of figure 6. At Mach numbers below 0.95, there is little or no change in pitching-moment coefficient at low lift coefficients due to flap deflection. However figure 6 shows that large increments in pitching-moment coefficient resulted from flap deflection for the horizontal-tail-on configurations. The results indicate that the high tail in conjunction with the deflected flaps makes an important contribution to the pitching-moment increment at Mach numbers below $M = 0.95$. The beneficial effect of the high tail in inducing an increment in pitching-moment coefficient can be attributed to increased downwash at the tail due to flap deflection. The increased downwash results in a more negative tail load with a resultant incremental pitching-moment coefficient.

Transonic Transport Model

Figures 9 and 10 show the effect of deflected flaps on the aerodynamic characteristics of the transport model for the tail-on condition. Figure 9 shows that the longitudinal location of the flap is important in obtaining an effective flap configuration. A flap located at the 0.65-chord line provided a lift increment at all Mach numbers; whereas, a flap of approximately the same deflection located at the 0.30-chord line gave little or no lift increment. The configuration with the 0.65-chord-line flap also gave increments in pitching-moment coefficient at lift coefficients from about $C_L = 0.1$ to about $C_L = 0.5$. However, negative increments in pitching-moment coefficient were provided by the configuration with the 0.30-chord-line flap, which would make the flap ineffective as a dive-recovery device. The configuration with the unswept flap located at $0.80c_r$ and deflected 90° gave little or no increments in lift or pitching-moment coefficients at all Mach numbers. (See fig. 10.)

Figures 11 and 12 show the effect of deflected-flap location on the aerodynamic characteristics of the model for the horizontal-tail-off condition. Figure 11 shows that both swept-flap configurations gave an increment in pitching-moment coefficient at all Mach numbers. However, the configuration having the 0.30-chord-line flap gave a decrement in pitching-moment coefficient at all Mach numbers for the tail-on

condition of figure 9. Redistribution of the wing loading, both chordwise and spanwise, due to flap deflection could cause the pitching-moment-coefficient changes shown in figures 9 and 11; however, the exact cause cannot be established conclusively in the absence of wing-loading data. The configuration with the 0.65-chord-line flap gave lift-coefficient and pitching-moment-coefficient increments for the tail-off case (fig. 11) that are not much different from the increments shown for the tail-on case (fig. 9). Comparison of the data of figure 12 with the data of figure 10 shows that the addition of the tail to the 0.80-root-chord-flap configuration resulted in decreased increments in pitching-moment coefficient. In view of the fact that small pitching-moment-coefficient increments, in addition to negative lift-coefficient increments, were obtained from the tests of the 0.50-root-chord-flap configuration (fig. 12), the configuration was not considered for tests with the tail on.

Of all the flap configurations tested on the transport model, only the configuration with the flap located at the 0.65-chord line appeared to be at all satisfactory as a dive-recovery device. Although this flap caused an increase in lift coefficient over the value for the basic model as shown in figure 11, no increment in pitching moment resulted from the addition of the tail as was observed for addition of the tail to the seaplane model. Part of this effect may be attributed to a redistribution of the wing loading, as was previously noted. However, it is believed that the location of the tail which was close to or in the wing wake may also have been a factor in the negligible contribution of the tail.

Pitching-Moment-Coefficient Increments

The change in pitching-moment coefficient at constant lift coefficient due to flap deflection $\Delta C_{m,t}$ is assumed to be a measure of the flap effectiveness, as was previously noted. A similar analysis in which this assumption has been made appears in reference 2. In actual practice, the initial change in pitching-moment coefficient at constant angle of attack due to flap deflection $\Delta C_{m,i}$ would also be important. This change in pitching-moment coefficient occurs when the flaps are deflected on an airplane and no trim correction is made in order to return the airplane to the initial lift coefficient. Thus, $\Delta C_{m,t}$ consists of $\Delta C_{m,i}$ plus a shift in pitching-moment coefficient required to return the airplane to the initial trim lift coefficient $\Delta C_{m,\Delta\alpha}$ or $\Delta C_{m,t} = \Delta C_{m,i} + \Delta C_{m,\Delta\alpha}$. The change in pitching-moment coefficient $\Delta C_{m,i}$ can be broken down into the change in wing pitching-moment coefficient (tail off) due to flap deflection at constant angle of attack

$\Delta C_{m,w}$ and the change in pitching-moment coefficient due to the change in tail loading caused by flap deflection at constant angle of attack $\Delta C_{m,D}$. The change in tail loading due to flap deflection is a result of the effect of wing downwash. Therefore, $\Delta C_{m,t} = \Delta C_{m,w} + \Delta C_{m,D} + \Delta C_{m,\Delta\alpha}$.

The effects of Mach number on the flap-effectiveness parameters $\Delta C_{m,t}$, $\Delta C_{m,w} + \Delta C_{m,D}$, $\Delta C_{m,w}$, $\Delta C_{m,\Delta\alpha}$, and $\Delta C_{m,D}$ at several values of lift coefficient are presented in figures 13 and 14. The additional lift coefficient ΔC_L due to flap deflection at constant angle of attack has also been presented because $\Delta C_{m,\Delta\alpha}$ is a function of the change in lift required to return the airplane to the initial lift coefficient.

Transonic seaplane model.- Figure 13 shows that the total incremental pitching-moment coefficients for the three flaps investigated, the 30° and 45° swept flaps and the 30° unswept flap, all have rather broad peaks which fall roughly in the Mach number range of 0.86 to 0.90 for lift coefficients of 0 to 0.40. Above $M = 0.90$ the curves generally fall with increasing Mach number. For $C_L = 0.60$, the total incremental pitching-moment coefficient is generally flat with Mach number variation for all three flaps. Figures 13(a) and 13(b) show that flap deflection on the model, at constant angle of attack, results in negative pitching-moment-coefficient contributions from the wing $\Delta C_{m,w}$ at Mach numbers below $M = 0.97$ for lift coefficients below $C_L = 0.40$. However, the large change in downwash due to flap deflection at these speeds nullifies the adverse effect of the wing pitching-moment contribution. The increment of pitching-moment coefficient due to downwash $\Delta C_{m,D}$ decreases with increase in Mach number and becomes practically zero at the highest Mach number reached, $M = 1.075$. This decrease of $\Delta C_{m,D}$ with increase in Mach number is overshadowed to some extent, at most lift coefficients, by an increase in the increment of pitching-moment coefficient made by the wing $\Delta C_{m,w}$.

Transonic transport model.- Figure 14 shows that the total incremental pitching-moment coefficients for the three flaps shown in the figure have rather broad peaks which fall roughly in the region of $M = 0.84$ to 0.88 in a manner similar to that for the seaplane model. Flap deflection on the transport model with horizontal tail off at constant angle of attack resulted in positive pitching-moment-coefficient changes for all three flaps and at all Mach numbers. These increments in pitching-moment coefficient remained relatively constant with increase in Mach number. The favorable effect of the flaps on the wing-body pitching moment is nullified in many instances by a negative contribution due to the wing downwash. This is particularly noticeable in

figure 14(b), for the 0.30-chord-line flap, where the effectiveness of the flap is completely overshadowed by the unfavorable downwash, so that the total pitching-moment change is negative.

CONCLUSION

From the results of a wind-tunnel investigation of the effects of dive-recovery flaps on models of a transonic seaplane and a transonic transport, both having swept wings, the following conclusions can be made:

1. With proper longitudinal location, wing-lower-surface dive-recovery flaps will produce lift and pitching-moment increments that increase with increased flap deflection.

2. For the transport model, a flap located aft on the wing lower surface proved more effective than one located more forward on the wing, both flaps having the same span and approximately the same deflection.

3. A high horizontal tail on the seaplane model provided added effectiveness for the deflected-flap configuration; whereas, on the transport model, a tail located slightly above the chord plane extended of the wing-body juncture generally gave a loss in effectiveness.

4. On the seaplane model, for a flap deflection of 30°, an unswept flap having a span of 26.7 percent of the wing semispan was as effective as a swept flap having a span of 35 percent of the wing semispan (both flaps had approximately the same longitudinal location).

Langley Research Center,
National Aeronautics and Space Administration,
Langley Field, Va., March 20, 1959.

REFERENCES

1. Mattson, Axel T.: Investigation of Dive Brakes and a Dive-Recovery Flap on a High-Aspect-Ratio Wing in the Langley 8-Foot High-Speed Tunnel. NACA RM L6H28c, 1946.

2. Hamilton, William T., and Boddy, Lee E.: High-Speed Wind-Tunnel Tests of Dive-Recovery Flaps on a 0.3-Scale Model of the P-47D Airplane. NACA ACR 5D19, 1945.

3. Erickson, Albert L.: Wind-Tunnel Investigation of Devices For Improving the Diving Characteristics of Airplanes. NACA MR 3F12, 1943.

4. Clarke, D. A.: High-Speed Tunnel Tests of a 5 percent Chord Dive-Recovery Flap on a NACA 0015 Aerofoil. R. & M. No. 2689, British A.R.C., 1953.

5. Ward, Vernon G., Whitcomb, Charles F., and Pearson, Merwin D.: Air-Flow and Power Characteristics of the Langley 16-Foot Transonic Tunnel With Slotted Test Section. NACA RM L52E01, 1952.

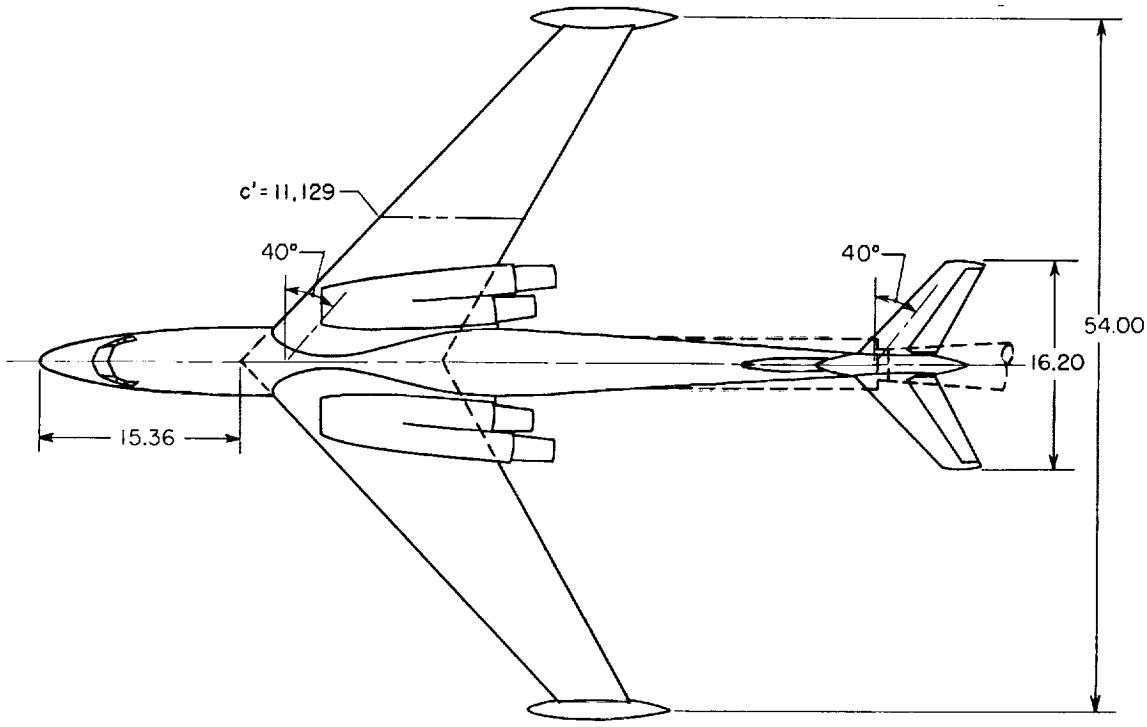

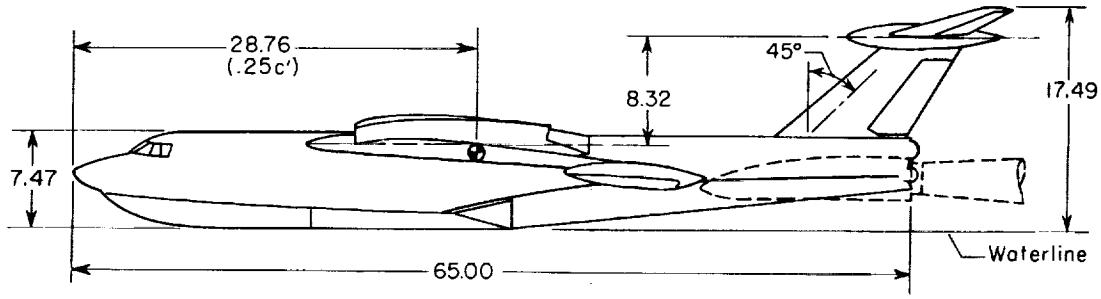

WING		HORIZONTAL TAIL	
Sections	NACA 63A3XX	Sections	NACA 63A009
Area, ft^2	3.852	Area, projected, ft^2	0.5214
AR	5.26	AR	3.5
Taper ratio	0.333	Taper ratio	0.4714
Sweep, c/4	40°	Sweep, c/4	40°

(a) Sketches of model. (All dimensions are in inches unless otherwise noted.)

Figure 1.- Transonic seaplane model.

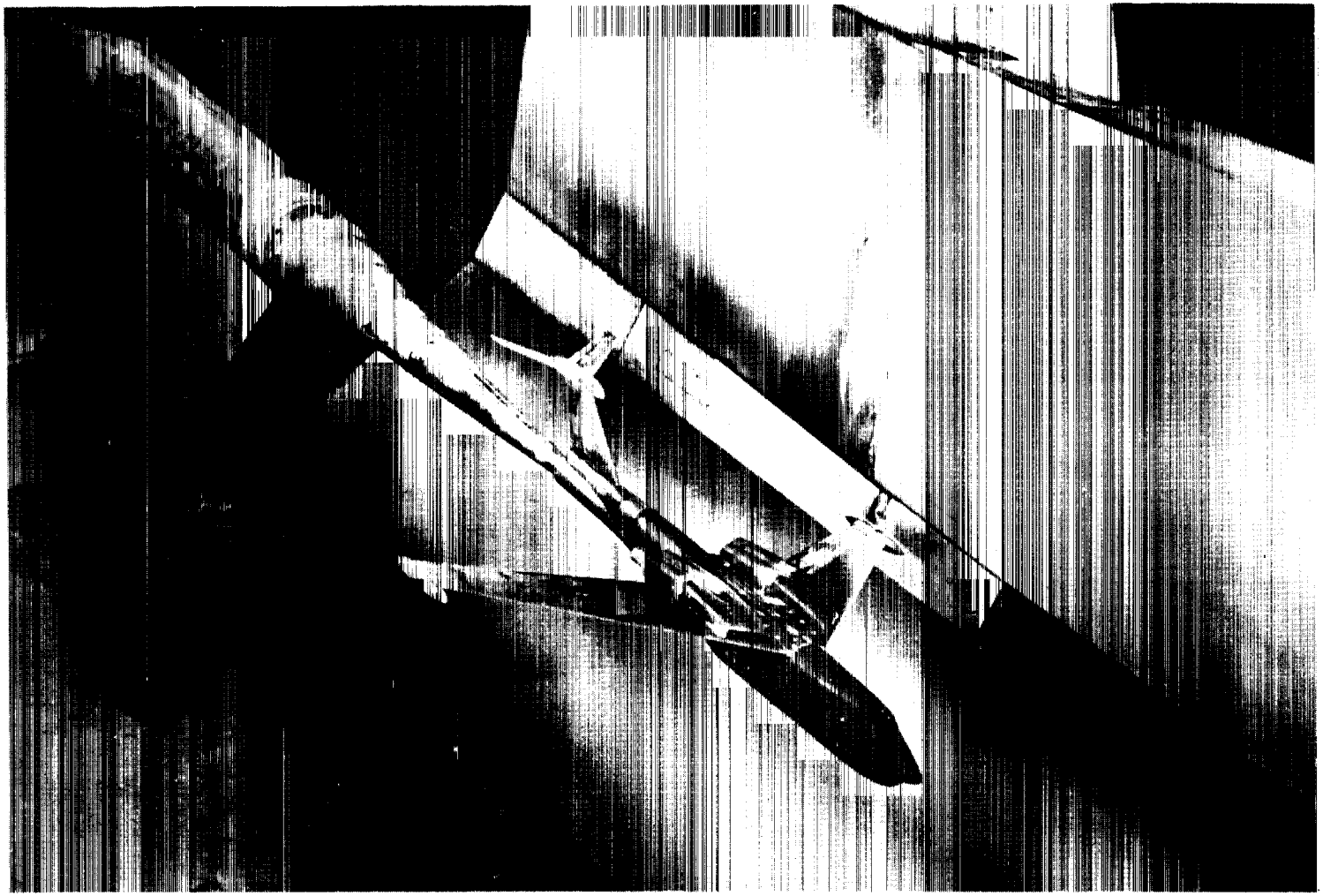

(b) Photograph of model in Langley 16-foot transonic tunnel. L-835421.1

Figure 1.- Concluded.

UNCLASSIFIED

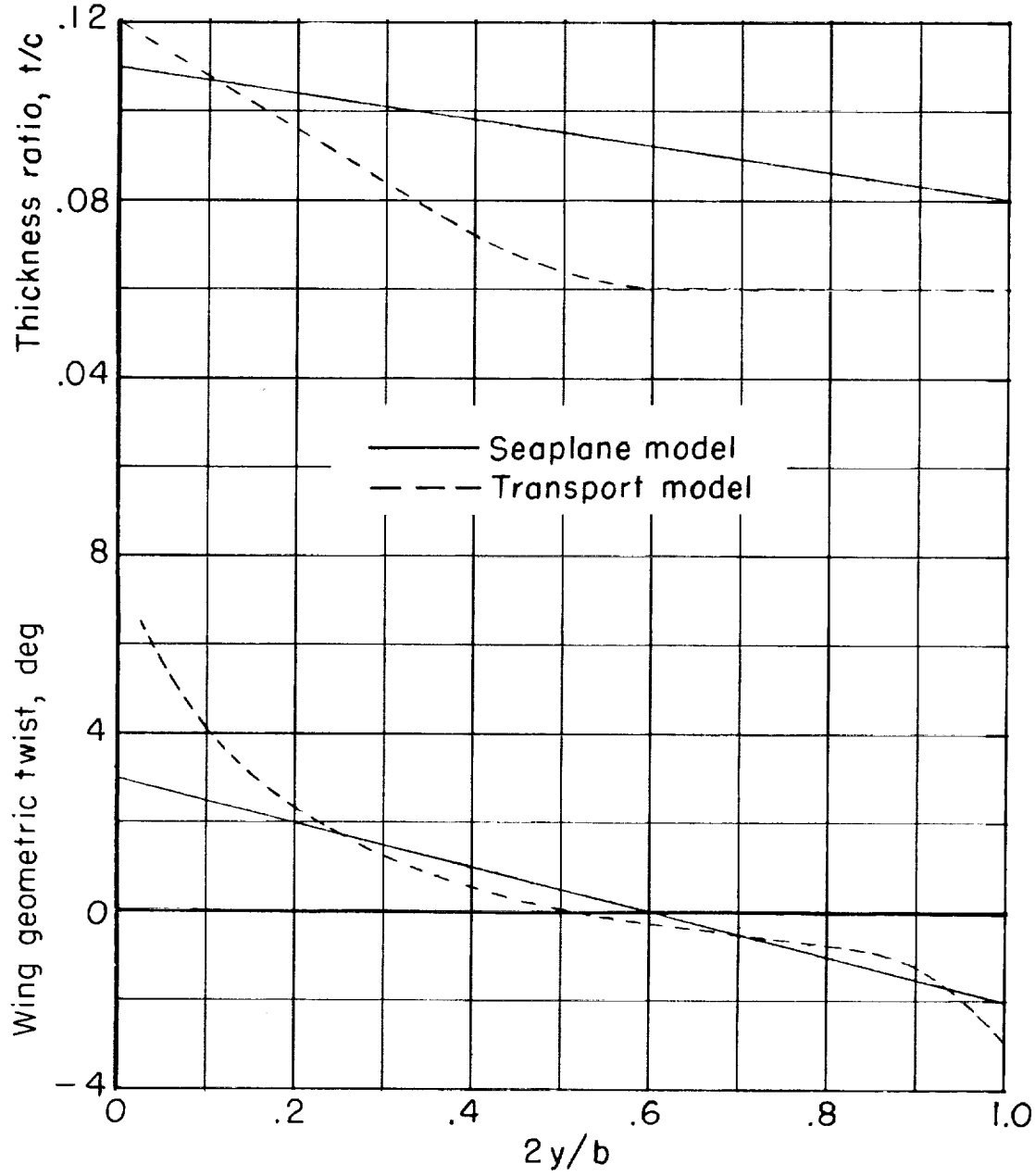

Figure 2.- Spanwise variation of thickness ratio and wing geometric twist of seaplane and transport models.

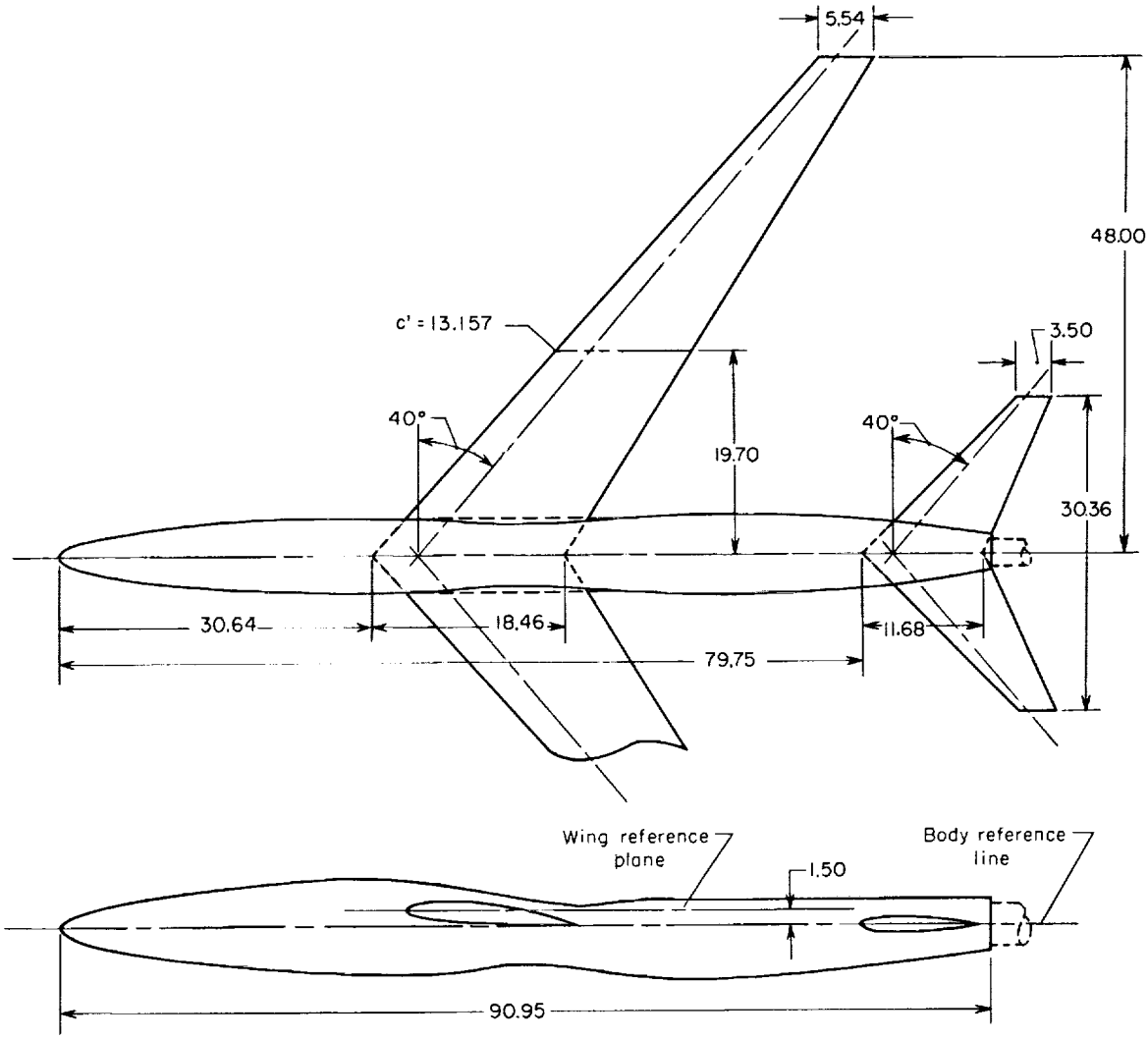

WING		HORIZONTAL TAIL	
Sections	NACA 65AXXX	Sections	NACA 65A006
Area, ft^2	8.0	Area, ft^2	1.6
AR	8.0	AR	4.0
Taper ratio	0.3	Taper ratio	0.3
Sweep, c/4	40°	Sweep, c/4	40°

(a) Sketches of model. (All dimensions are in inches unless otherwise noted.)

Figure 3.- Transonic transport model.

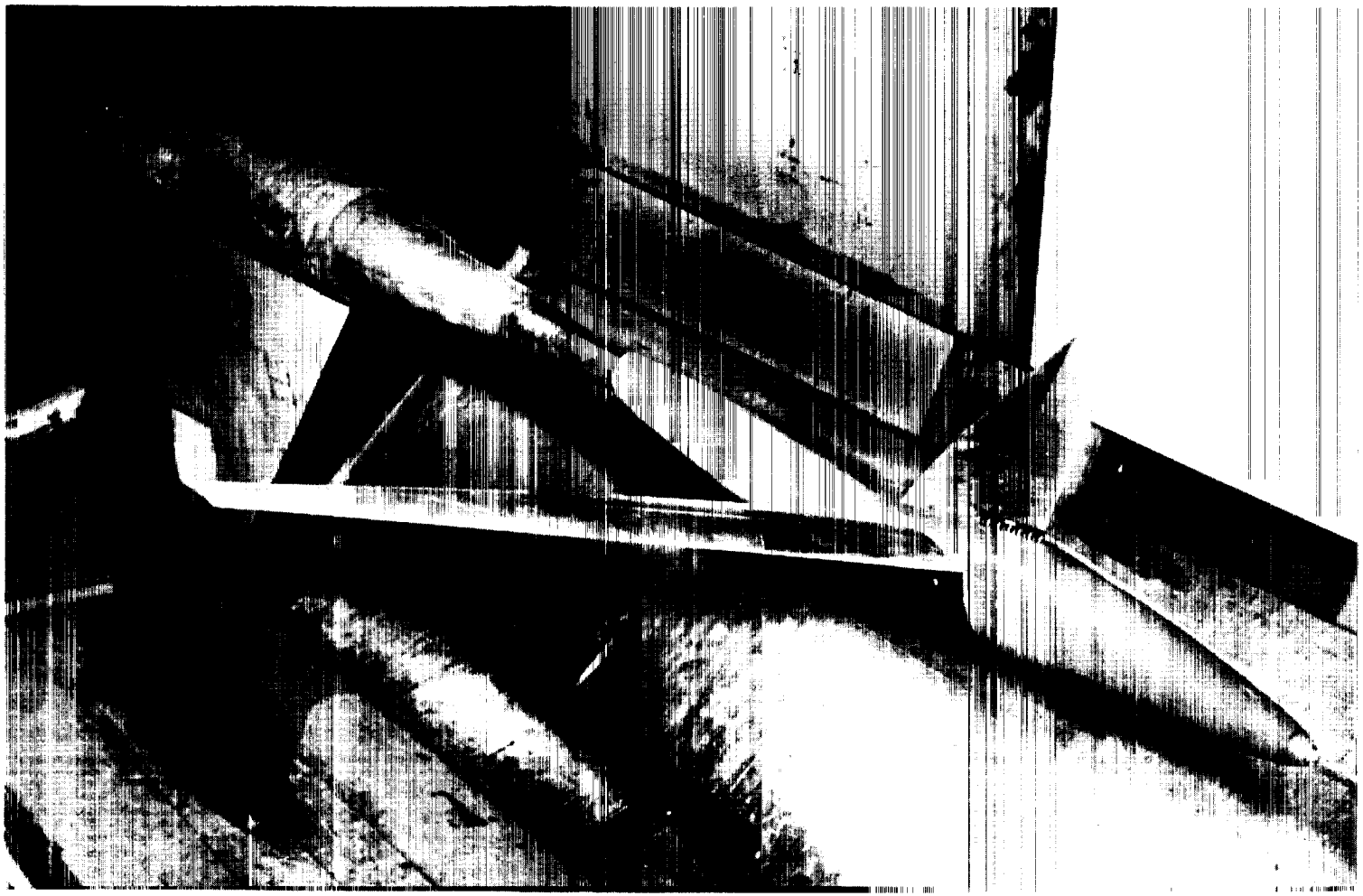

(b) Photograph of model in Langley 16-foot transonic tunnel. L-57-593

Figure 3.- Concluded.

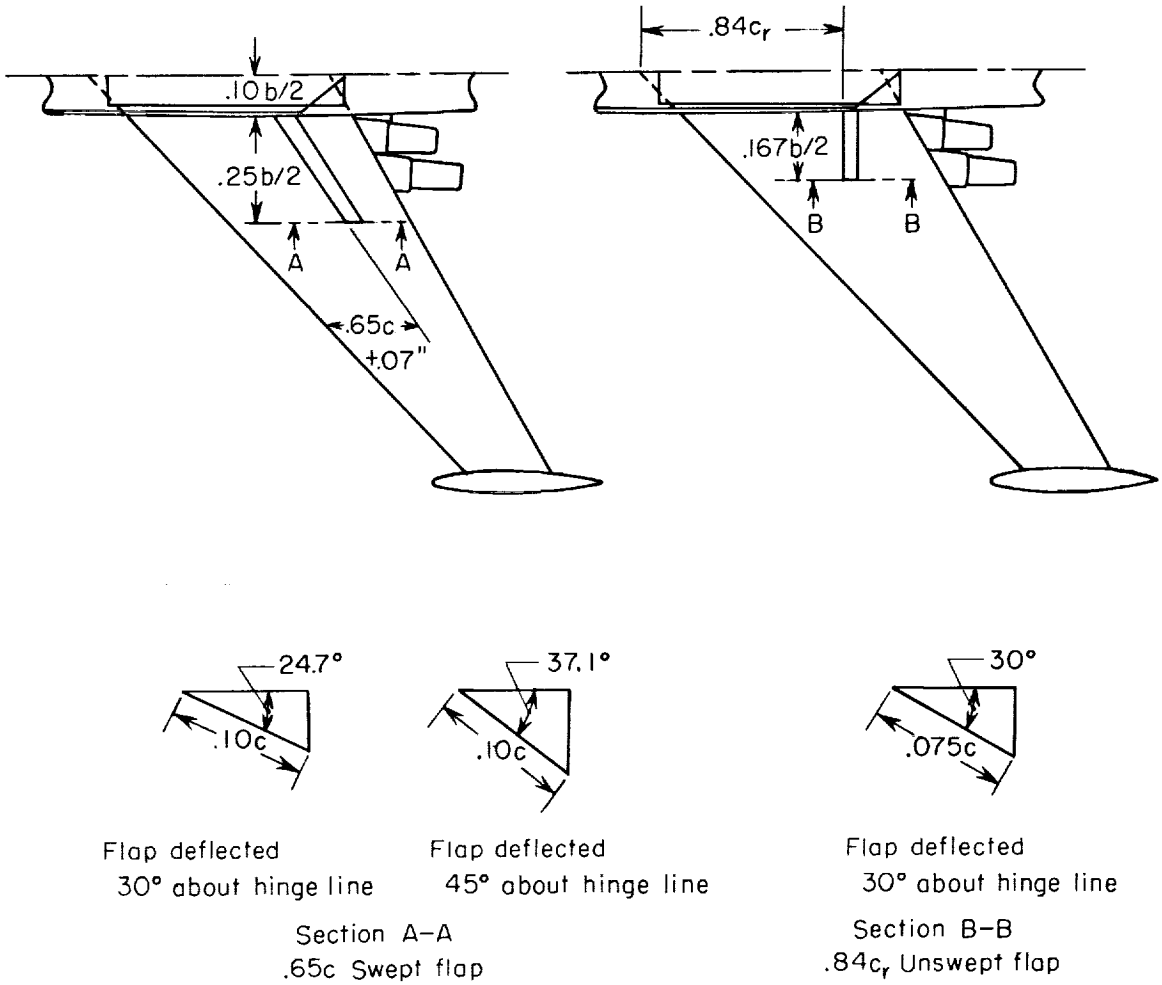

(a) Seaplane model.

Figure 4.- Sketches of dive-recovery flaps on lower surfaces of wings.

DECLASSIFIED

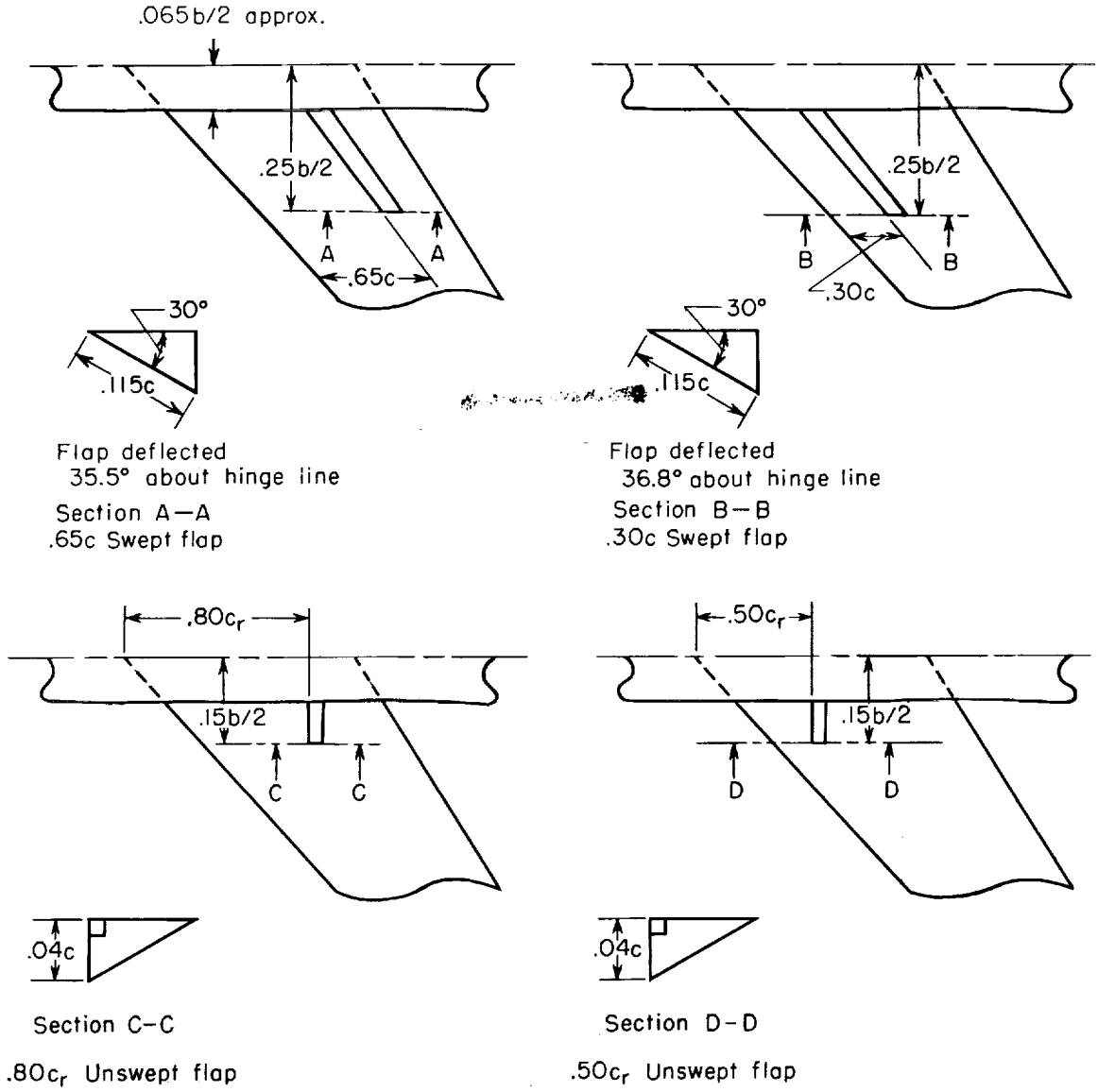

(b) Transport model.

Figure 4.- Concluded.

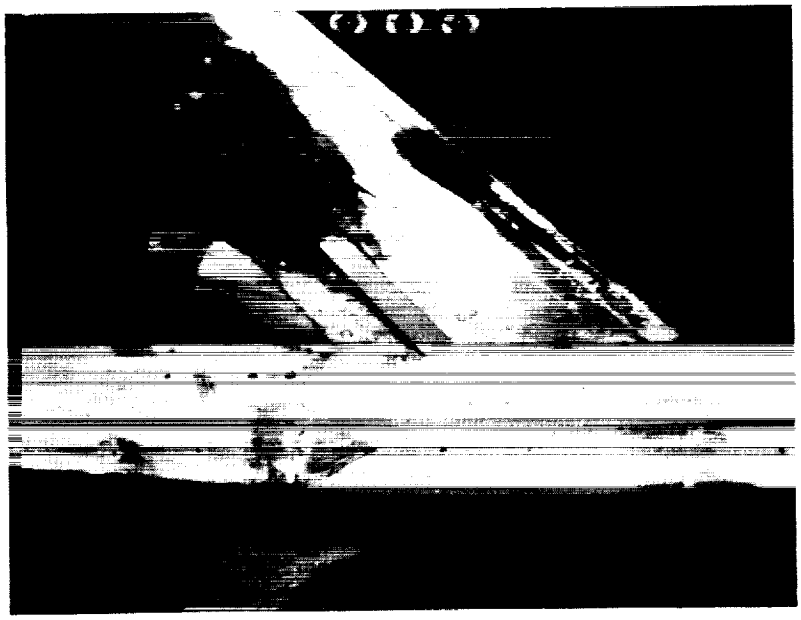

(a) Seaplane model. L-57-4643

(b) Transport model. L-57-4904

Figure 5.- Photographs of dive-recovery flaps installed on lower surfaces of wings.

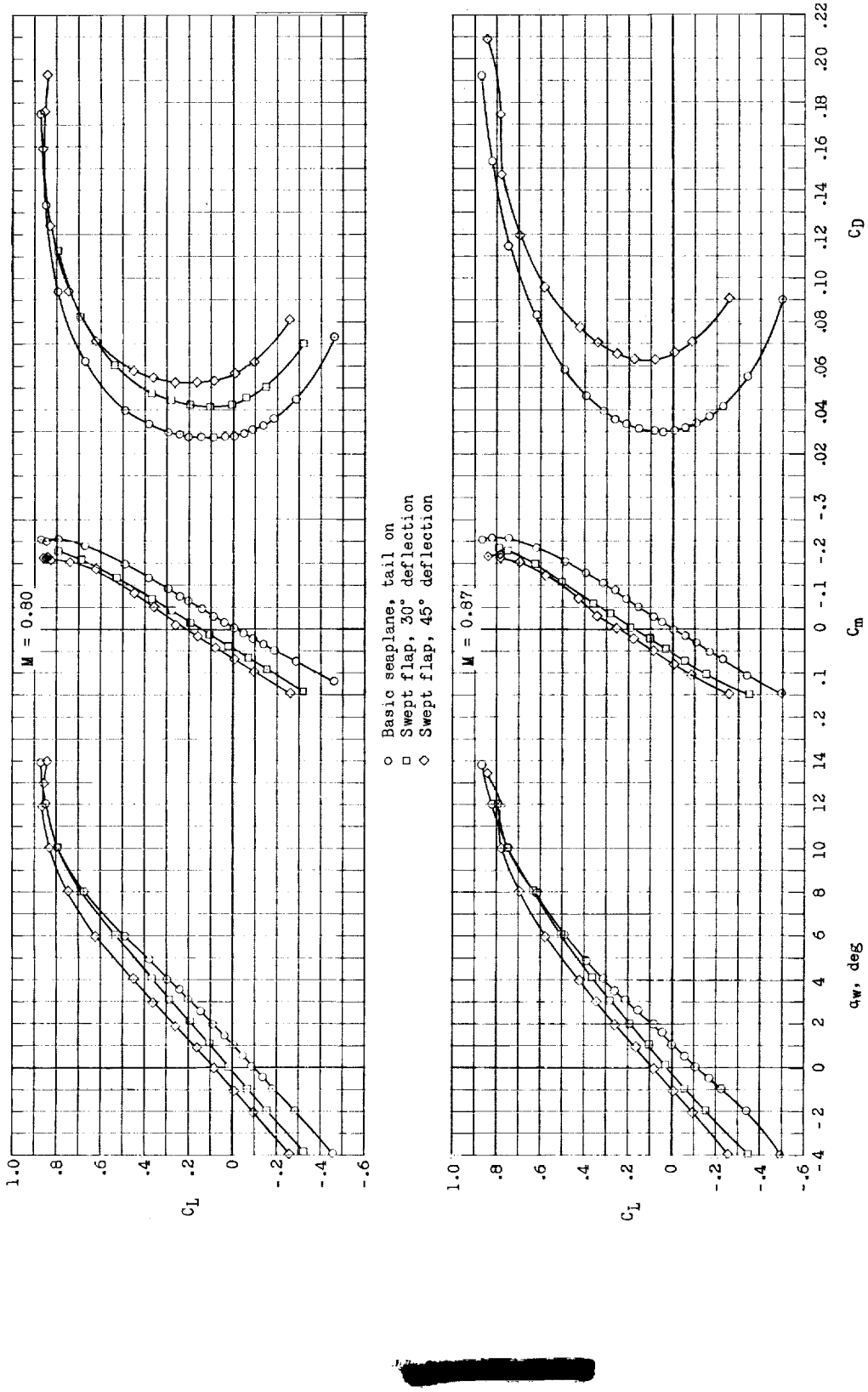

(a) M = 0.80 and 0.87.

Figure 6.- Effect of swept-flap deflections on longitudinal stability characteristics of seaplane model. Horizontal tail on.

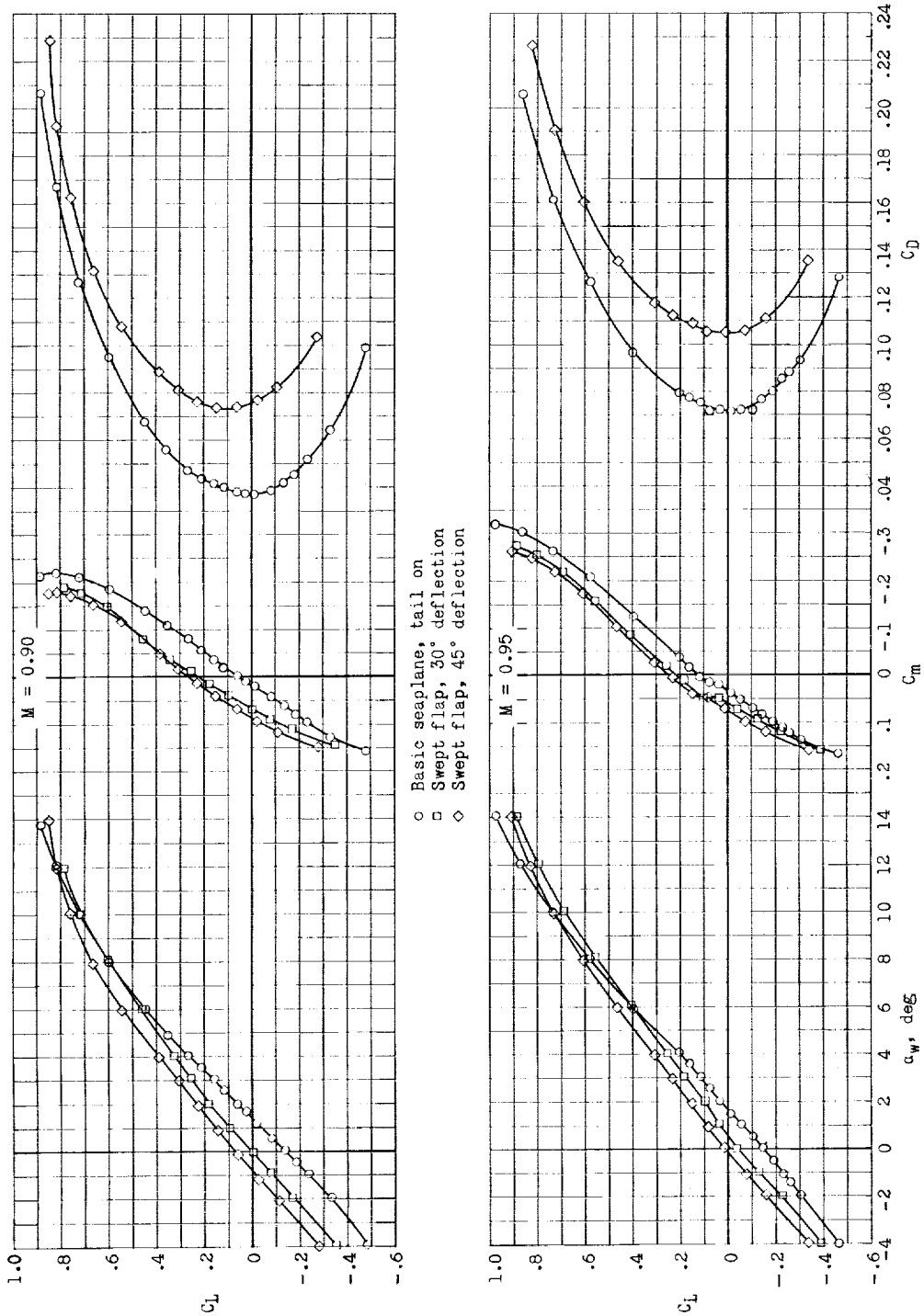

(b) M = 0.90 and 0.95.

Figure 6.- Continued.

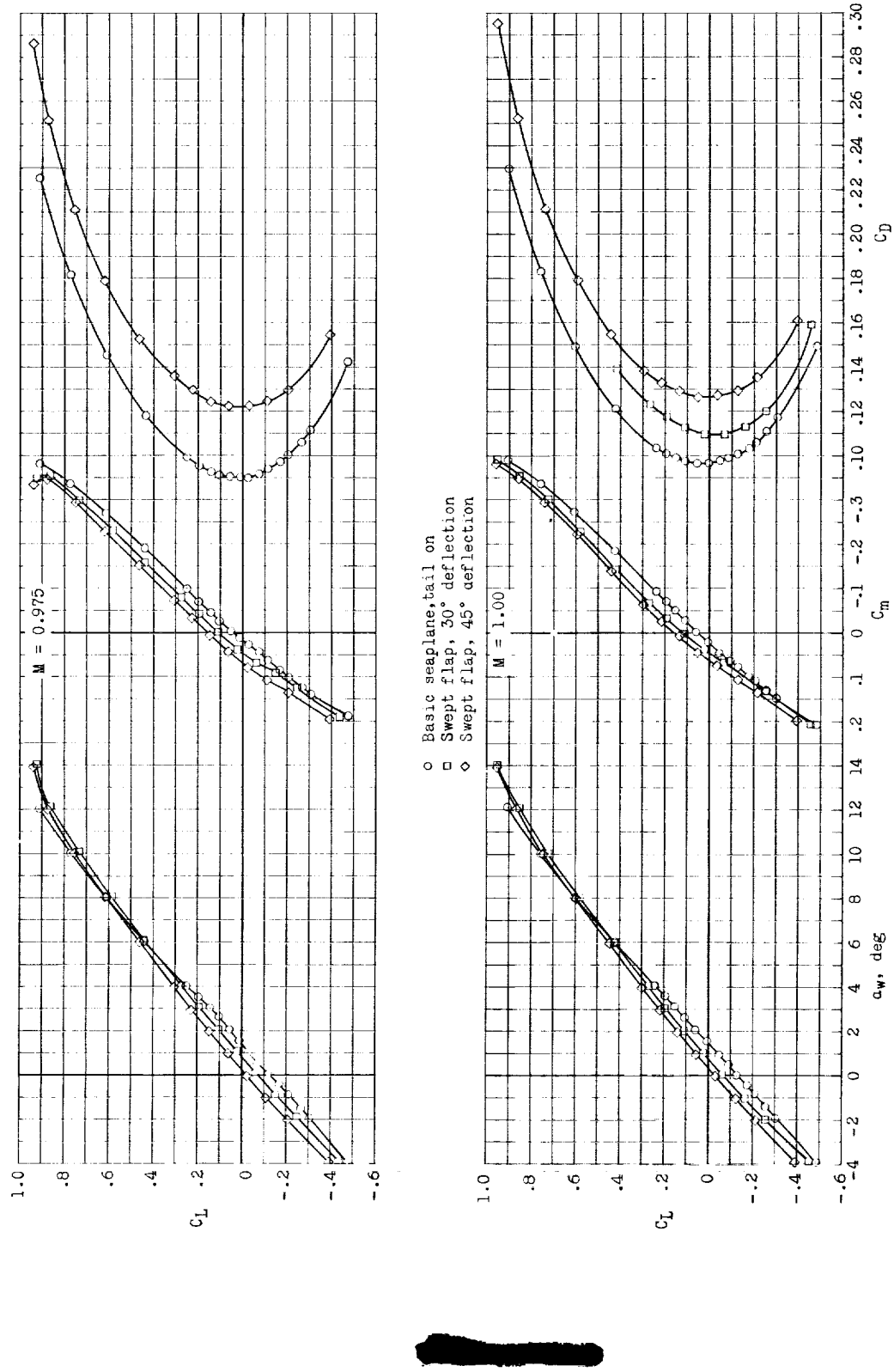

(c) M = 0.975 and 1.00.

Figure 6.- Continued.

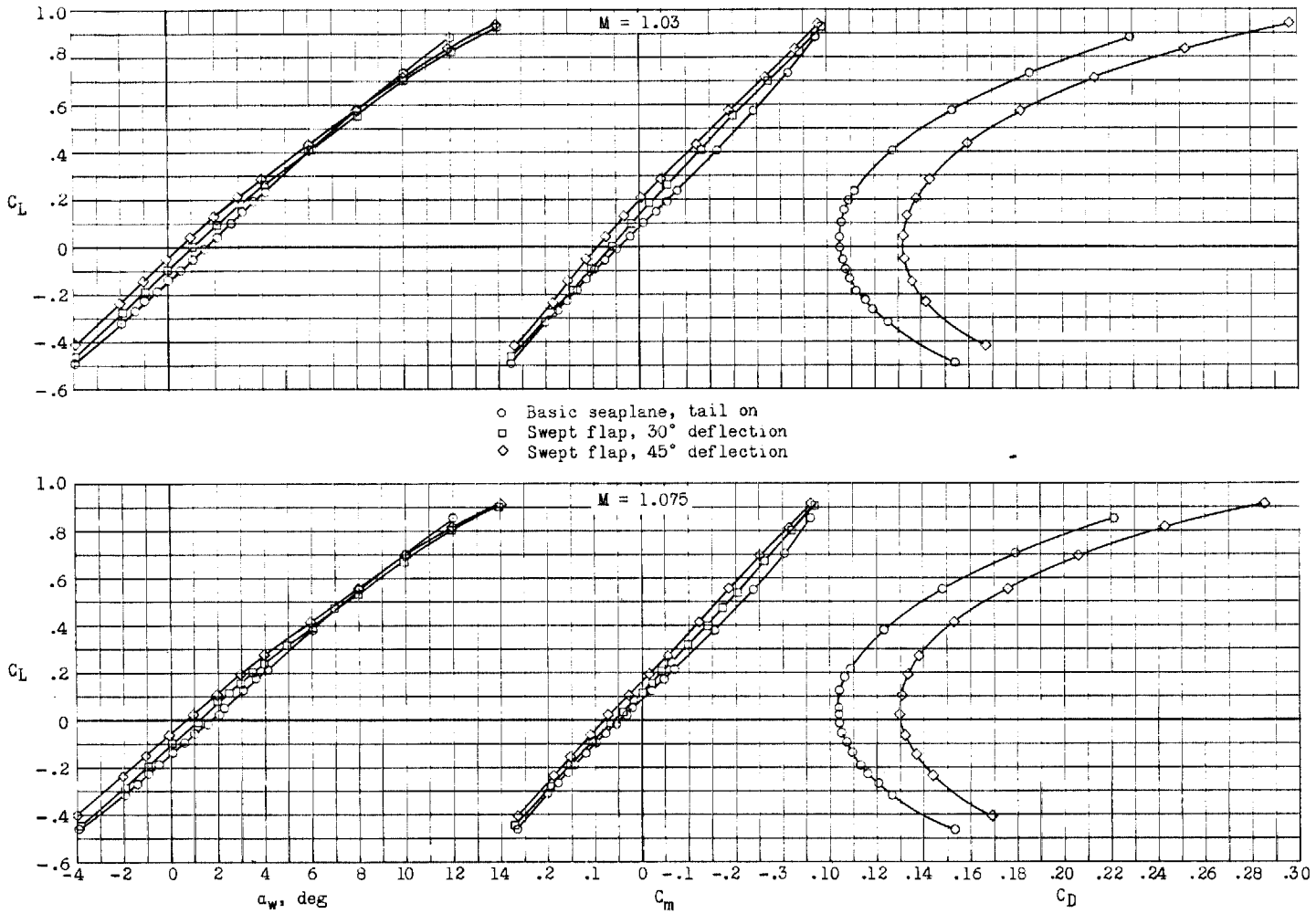

(d) M = 1.03 and 1.075.

Figure 6.- Concluded.

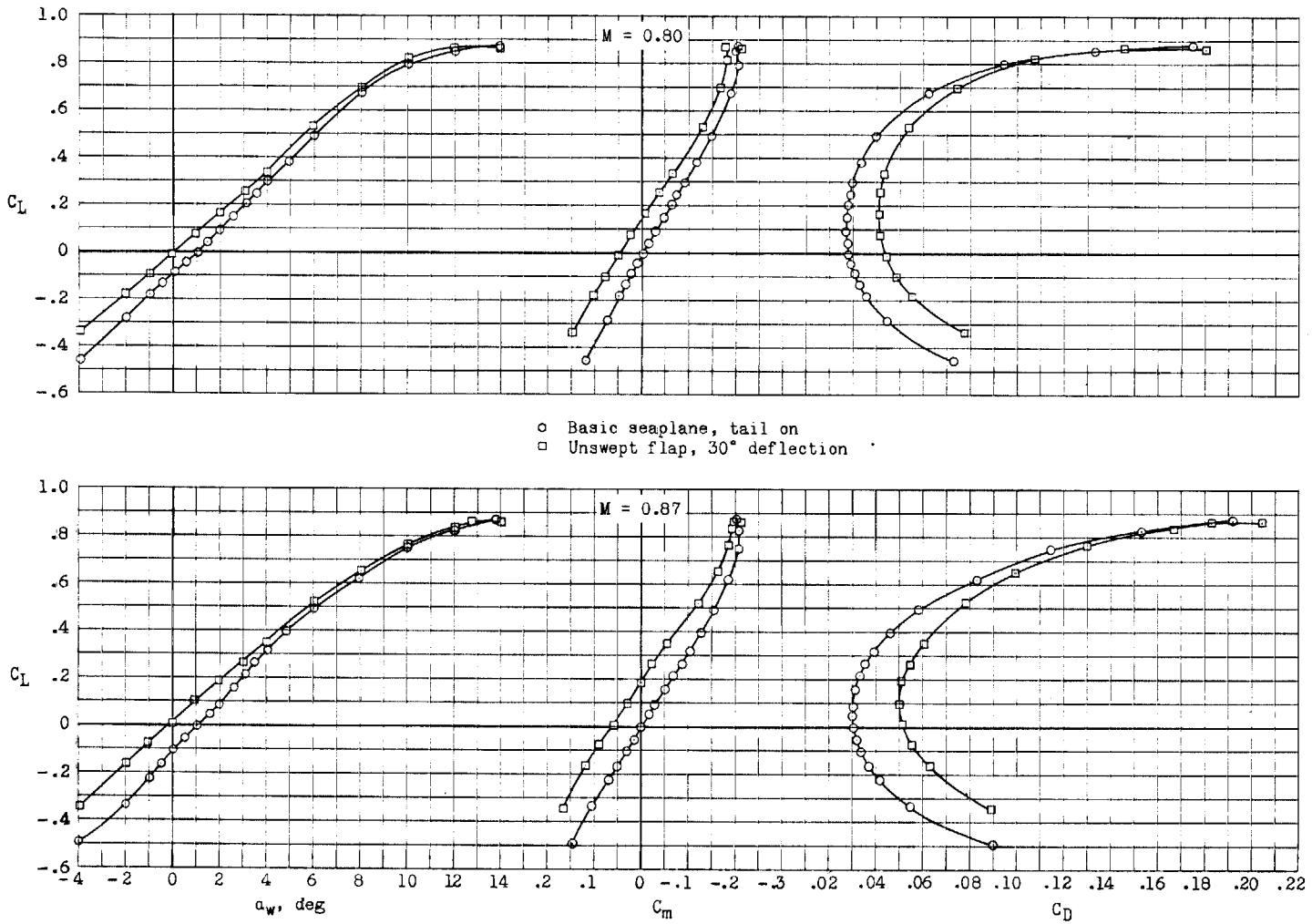

(a) M = 0.80 and 0.87.

Figure 7.- Effect of unswept-flap deflections on longitudinal stability characteristics of seaplane model. Horizontal tail on.

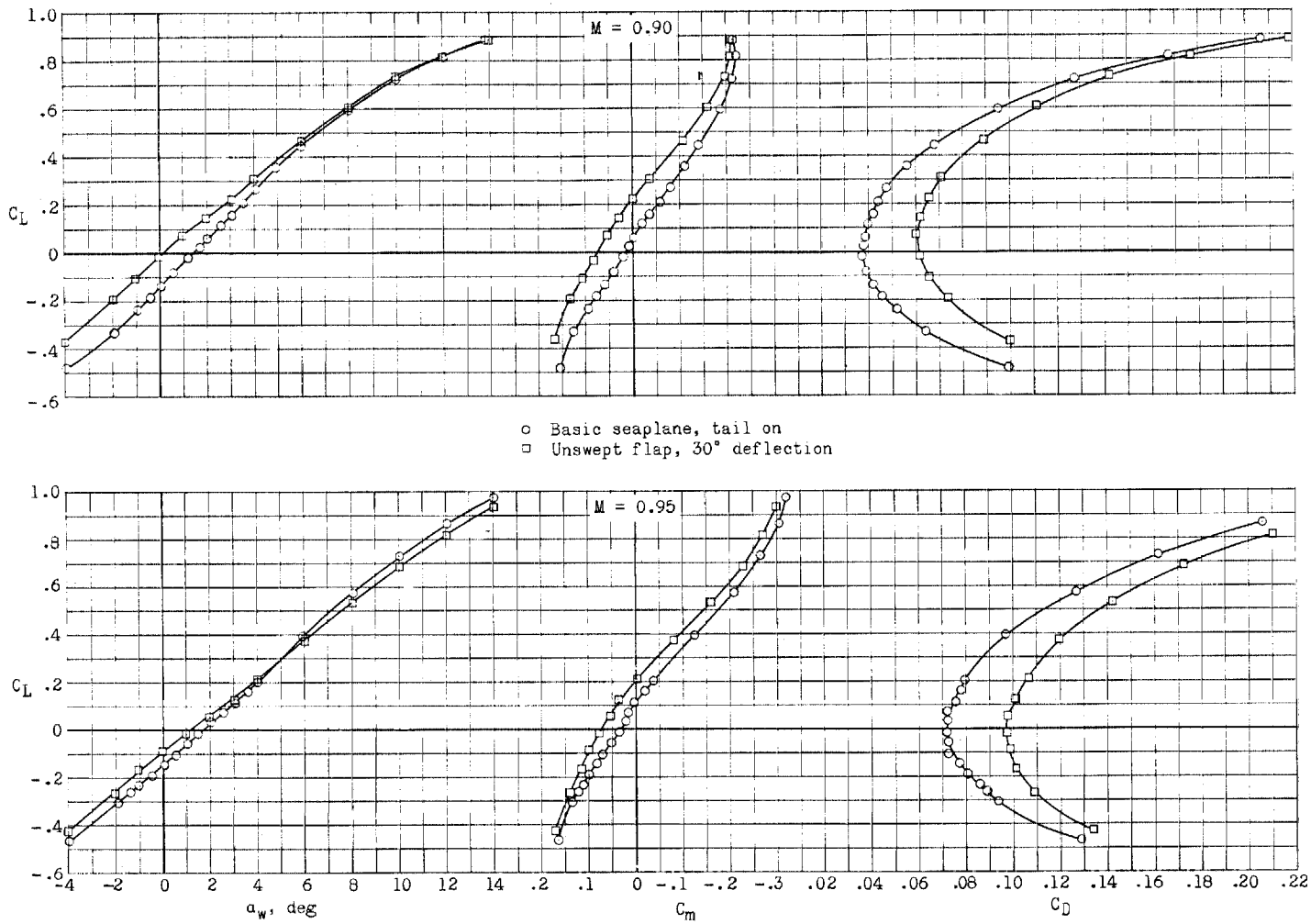

(b) M = 0.90 and 0.95.

Figure 7.- Continued.

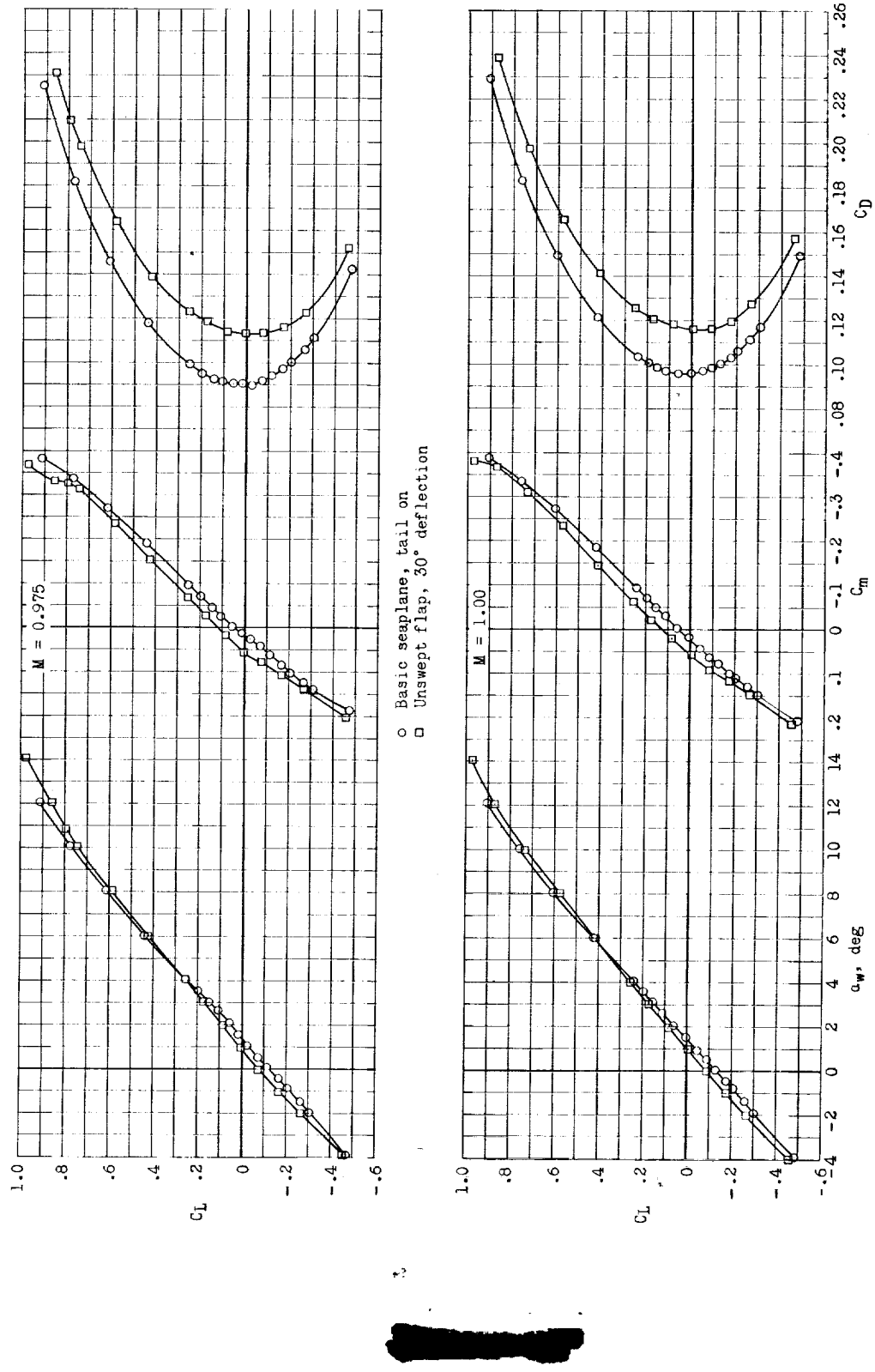

(c) M = 0.975 and 1.00.

Figure 7.- Continued.

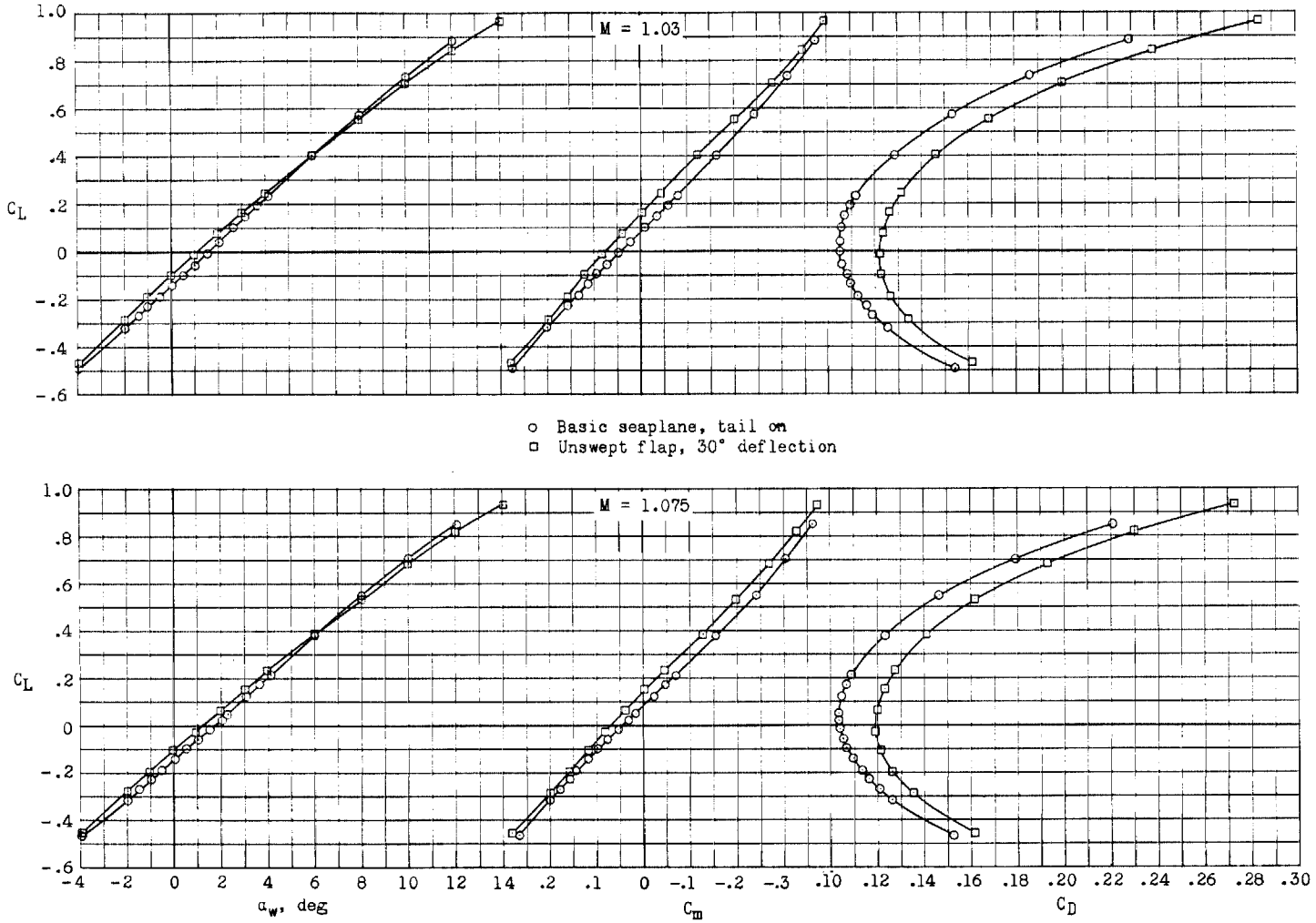

(d) M = 1.03 and 1.075.

Figure 7.- Concluded.

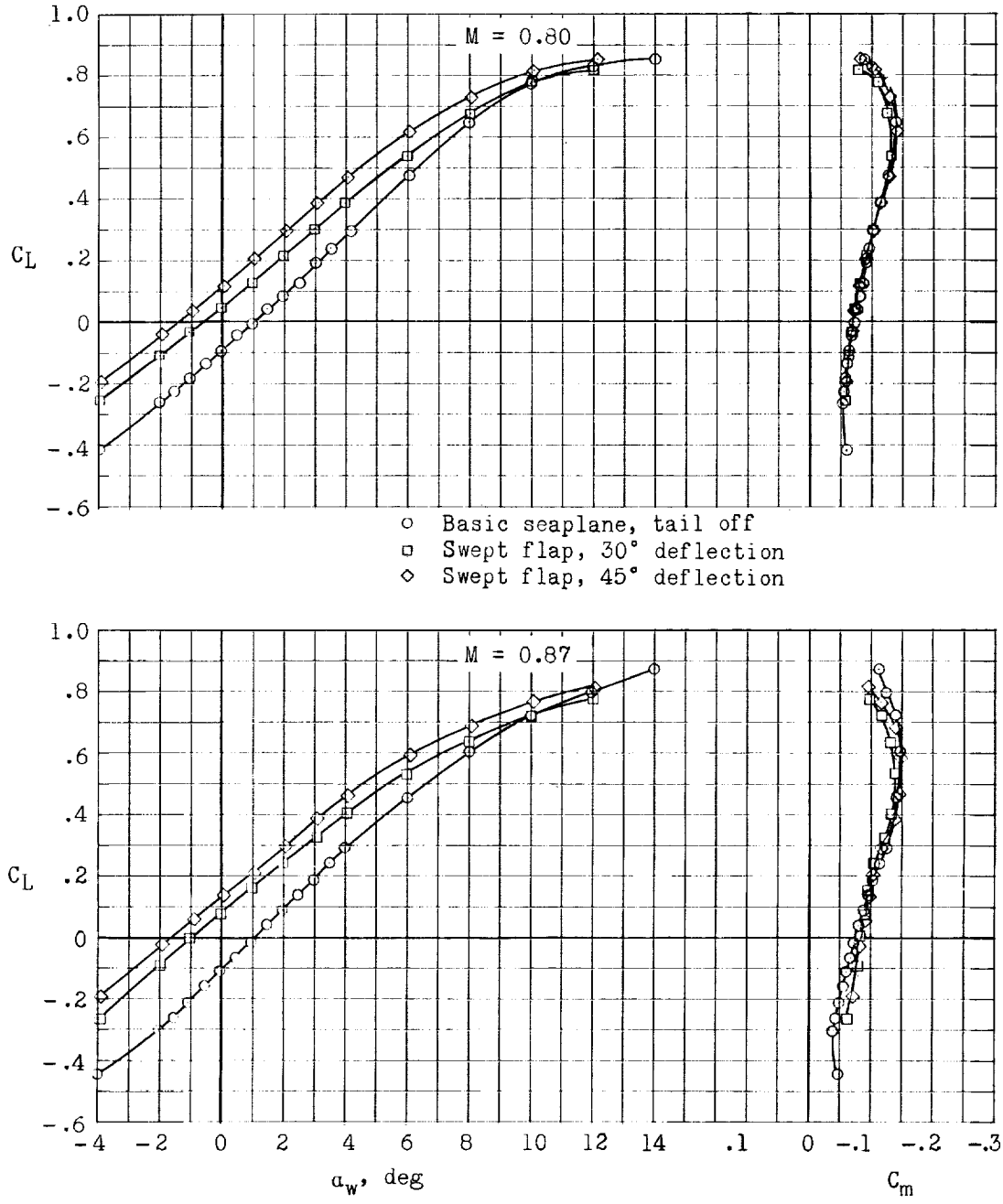

(a) M = 0.80 and 0.87.

Figure 8.- Effect of swept-flap deflections on longitudinal stability characteristics of seaplane model. Horizontal tail off.

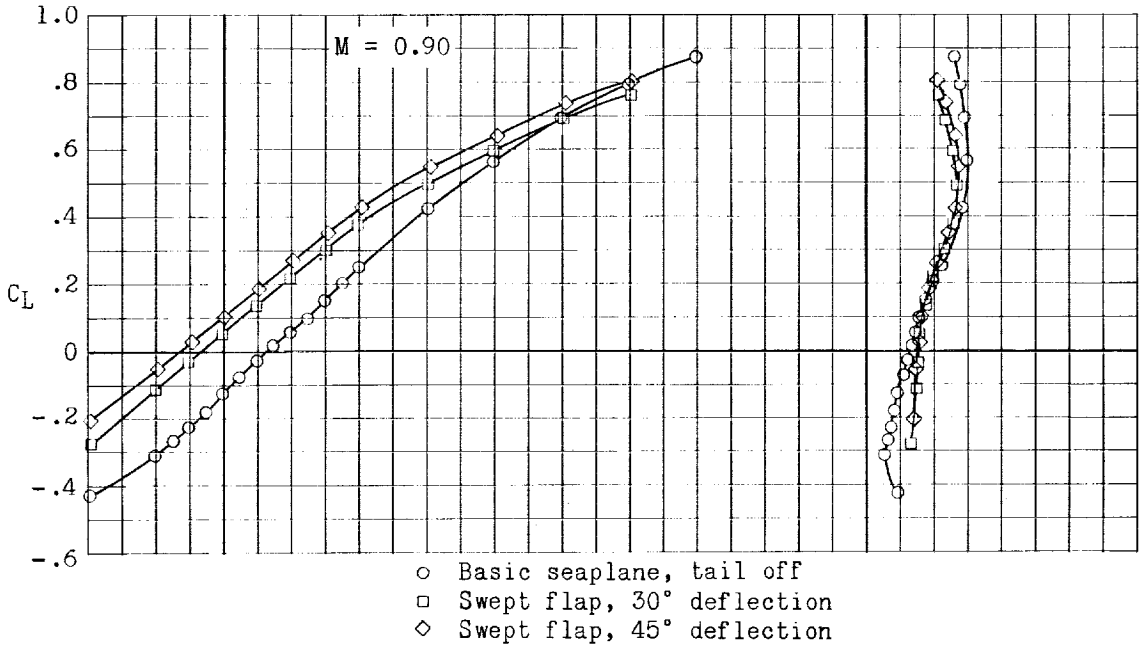

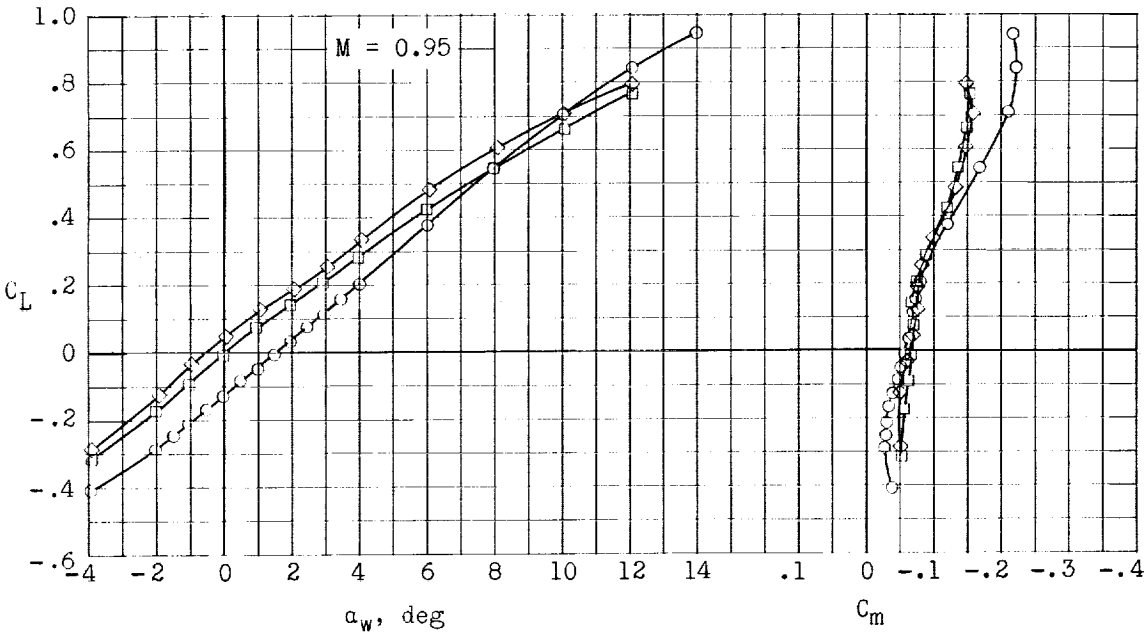

(b) M = 0.90 and 0.95.

Figure 8.- Continued.

[redacted]

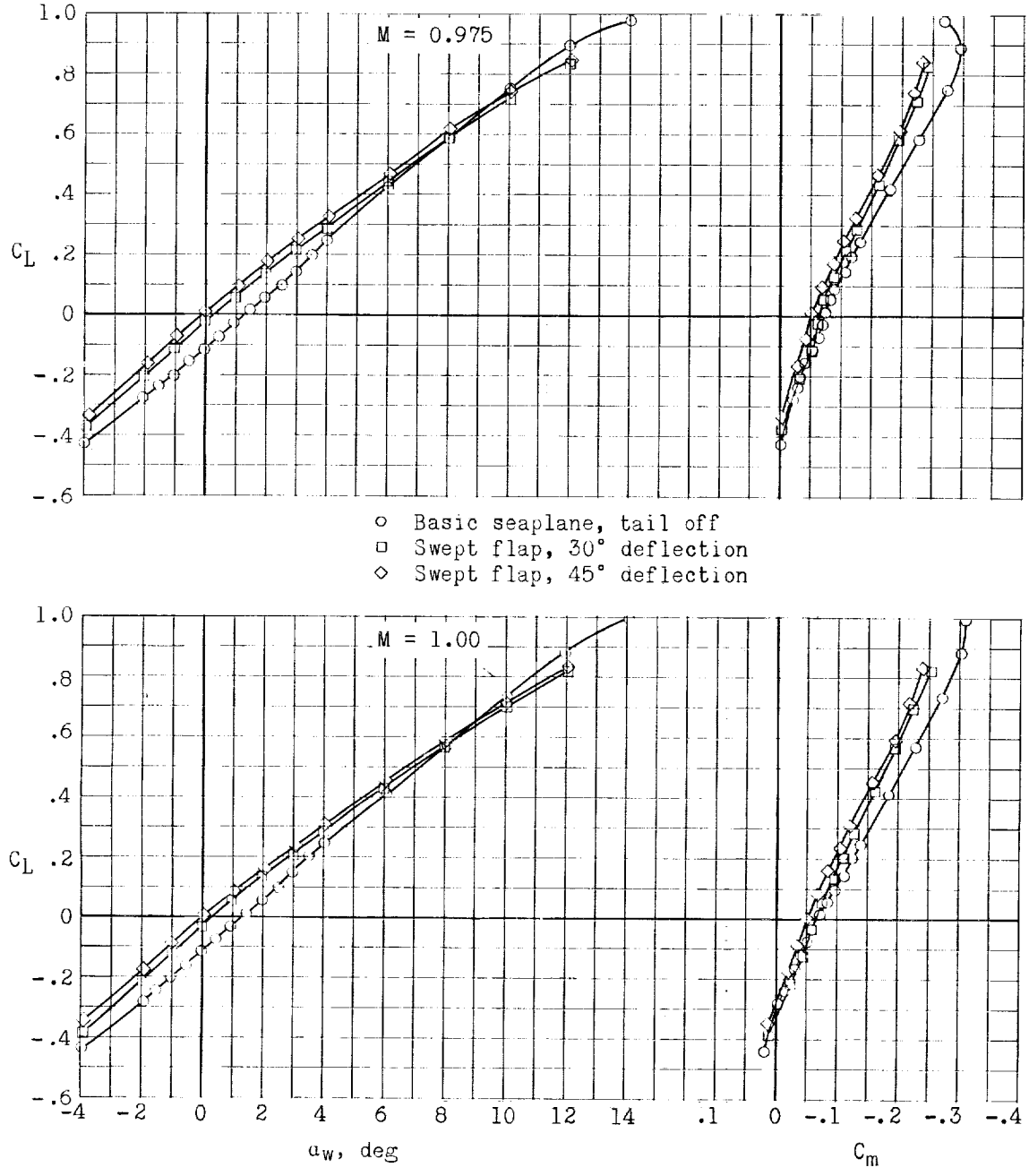

(c) M = 0.975 and 1.00.

Figure 8.- Continued.

[redacted]

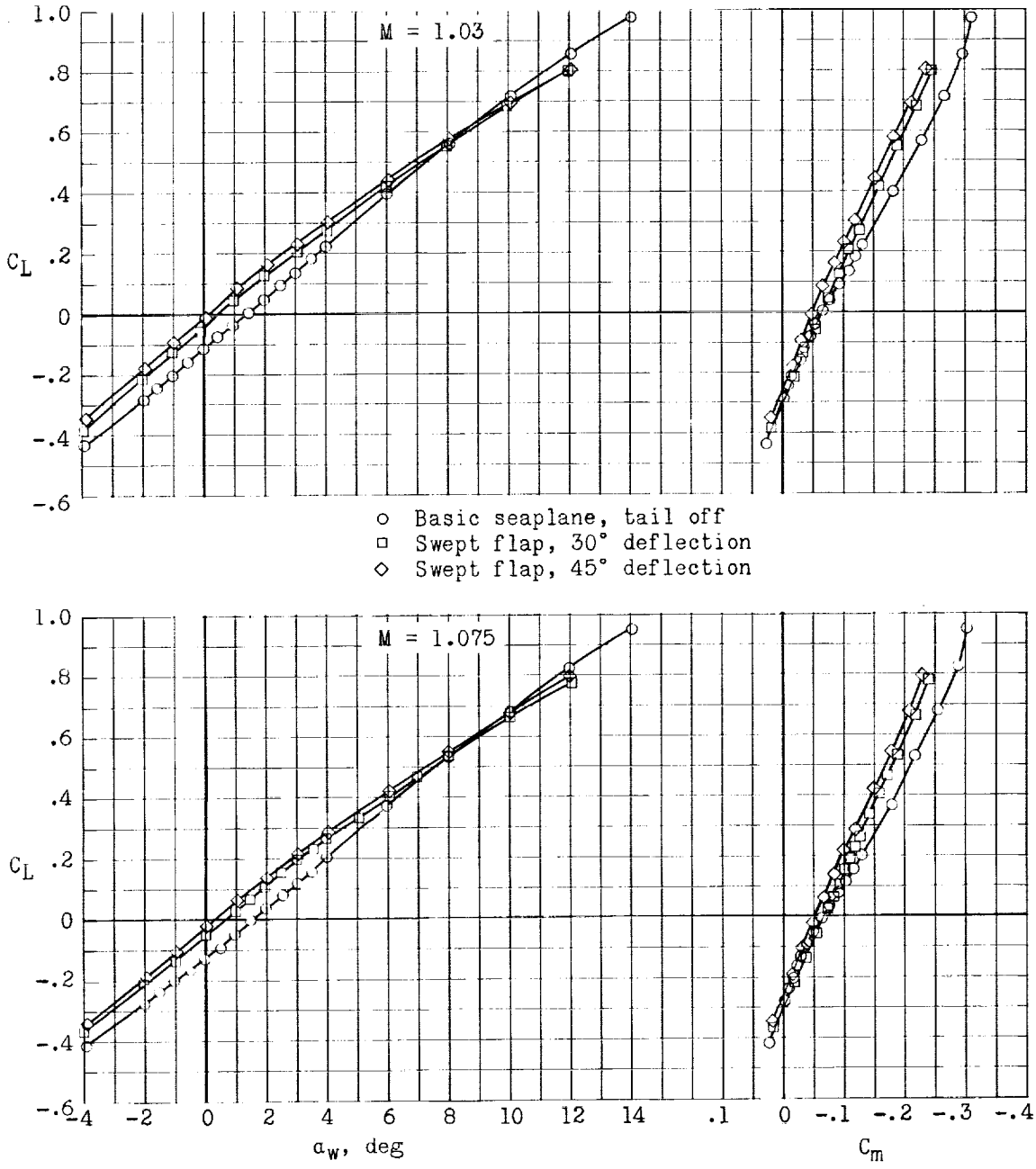

(d) M = 1.03 and 1.075.

Figure 8.- Concluded.

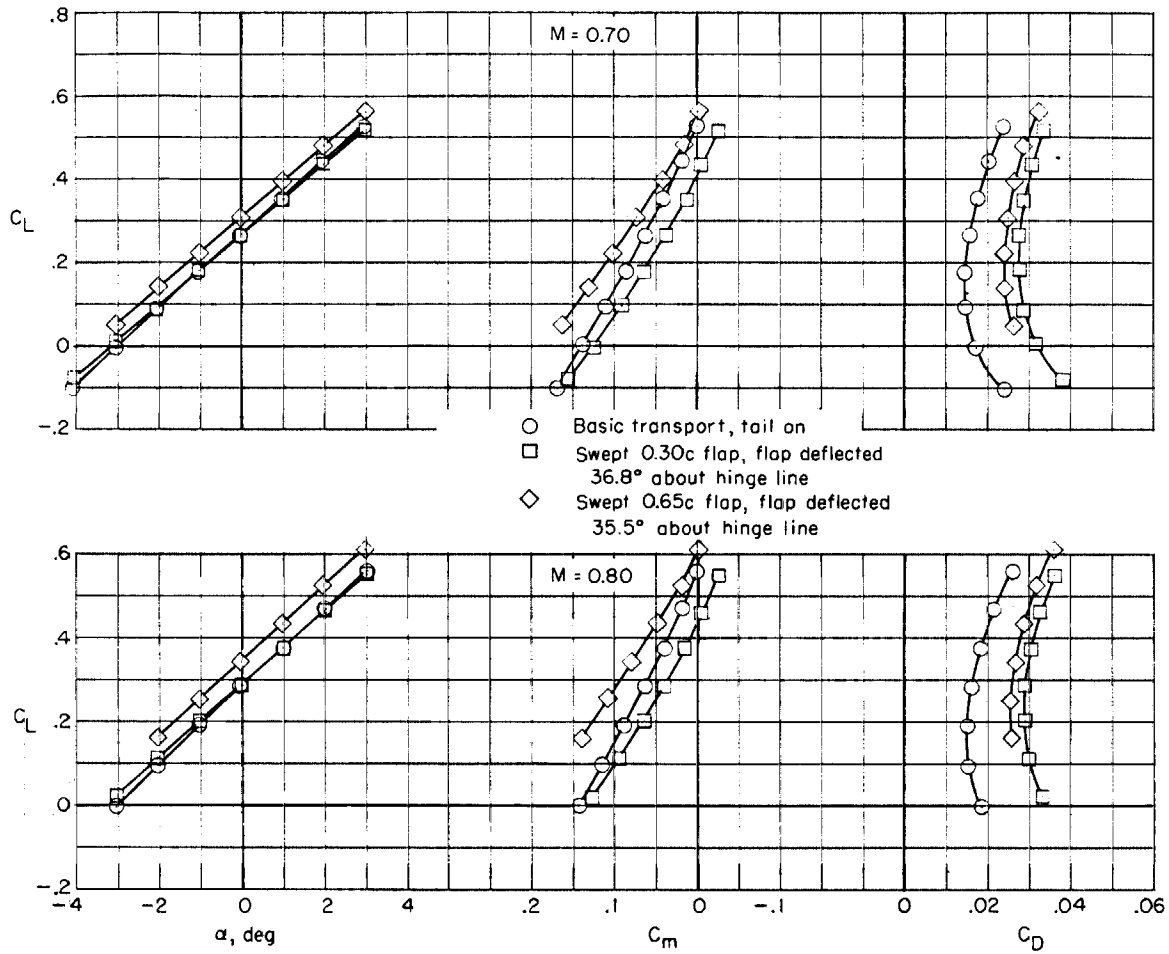

(a) M = 0.70 and 0.80.

Figure 9.- Effect of swept-flap locations on longitudinal stability characteristics of transport model. Horizontal tail on.

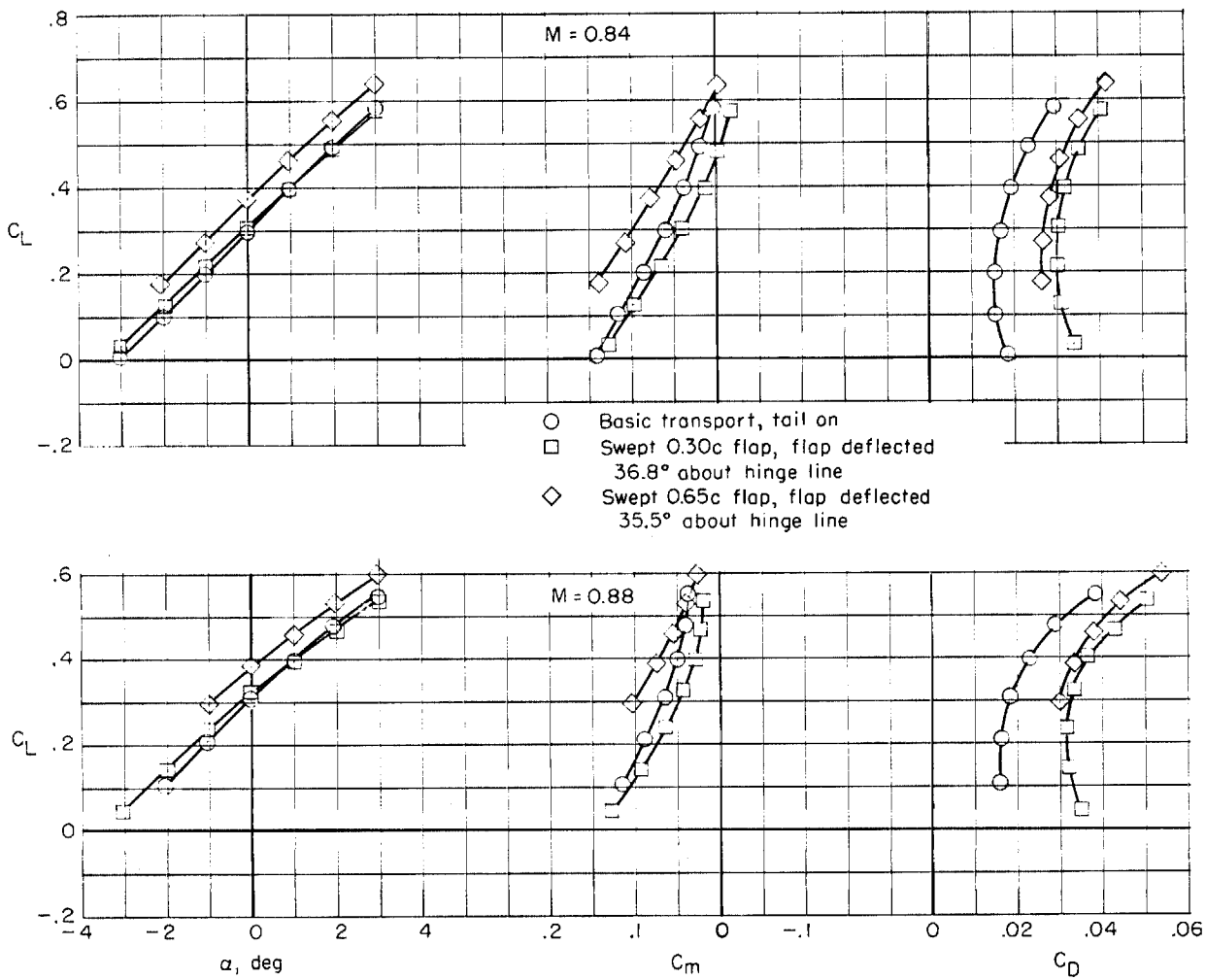

(b) M = 0.84 and 0.88.

Figure 9.- Continued.

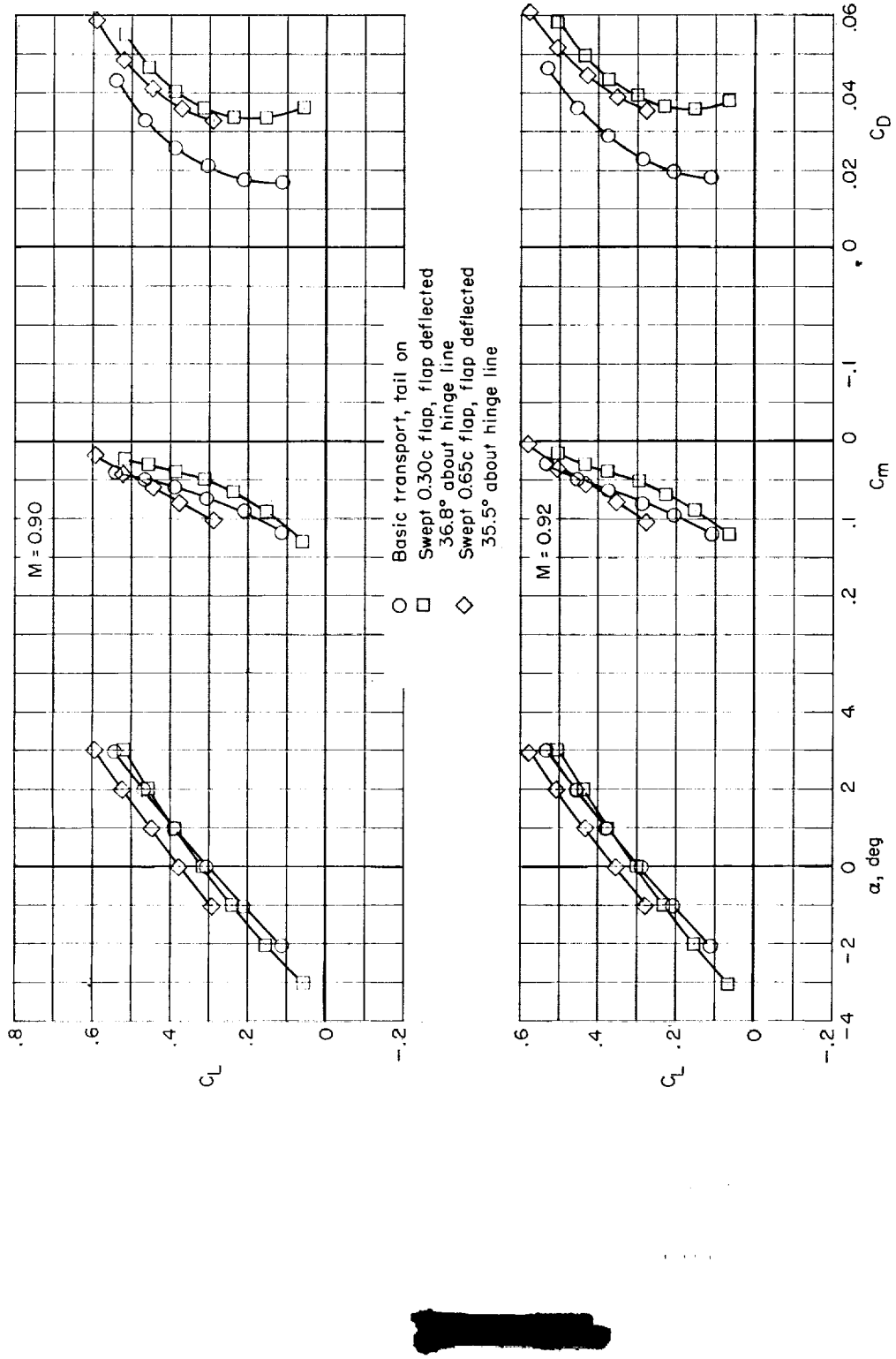

(c) M = 0.90 and 0.92.

Figure 9.- Concluded.

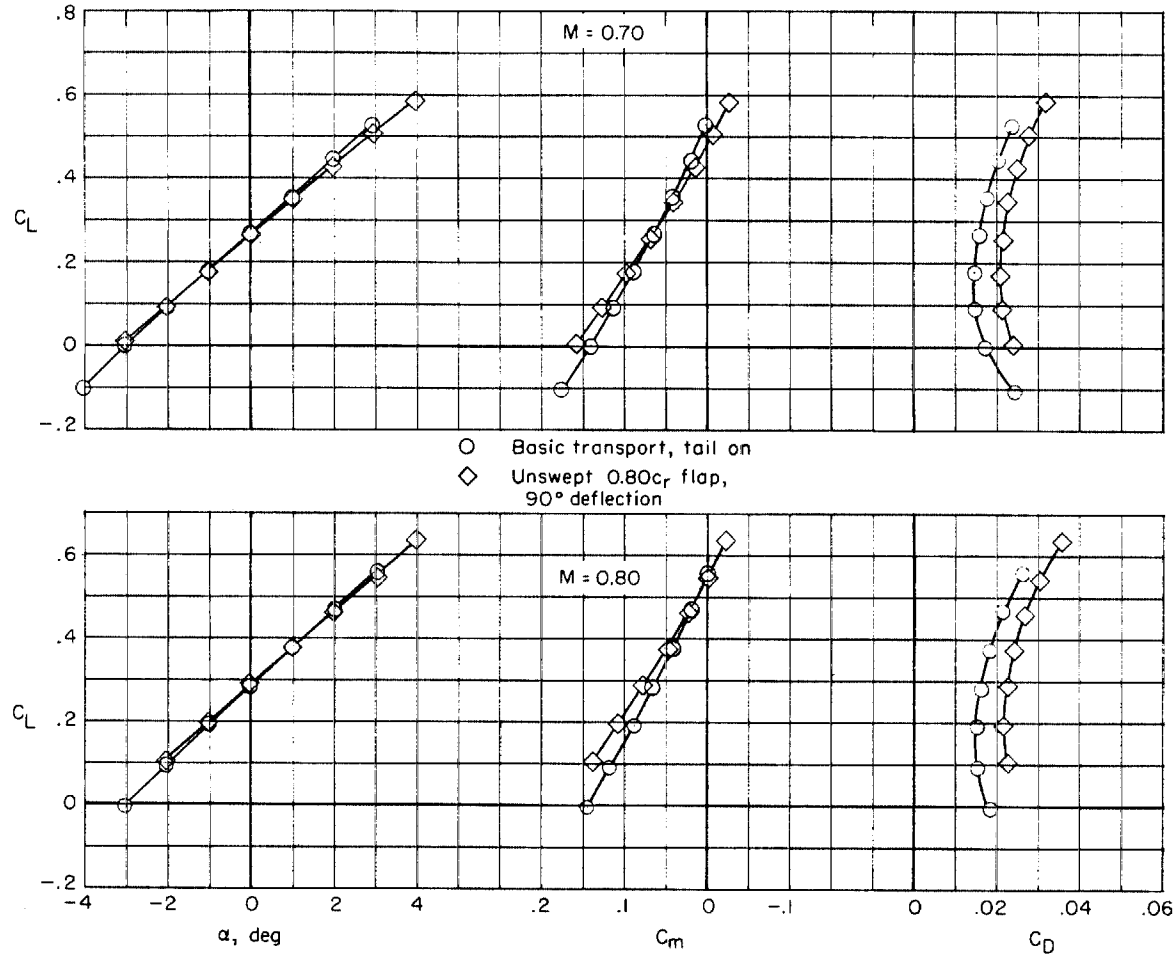

(a) M = 0.70 and 0.80.

Figure 10.- Effect of unswept-flap deflections on longitudinal stability characteristics of transport model. Horizontal tail on.

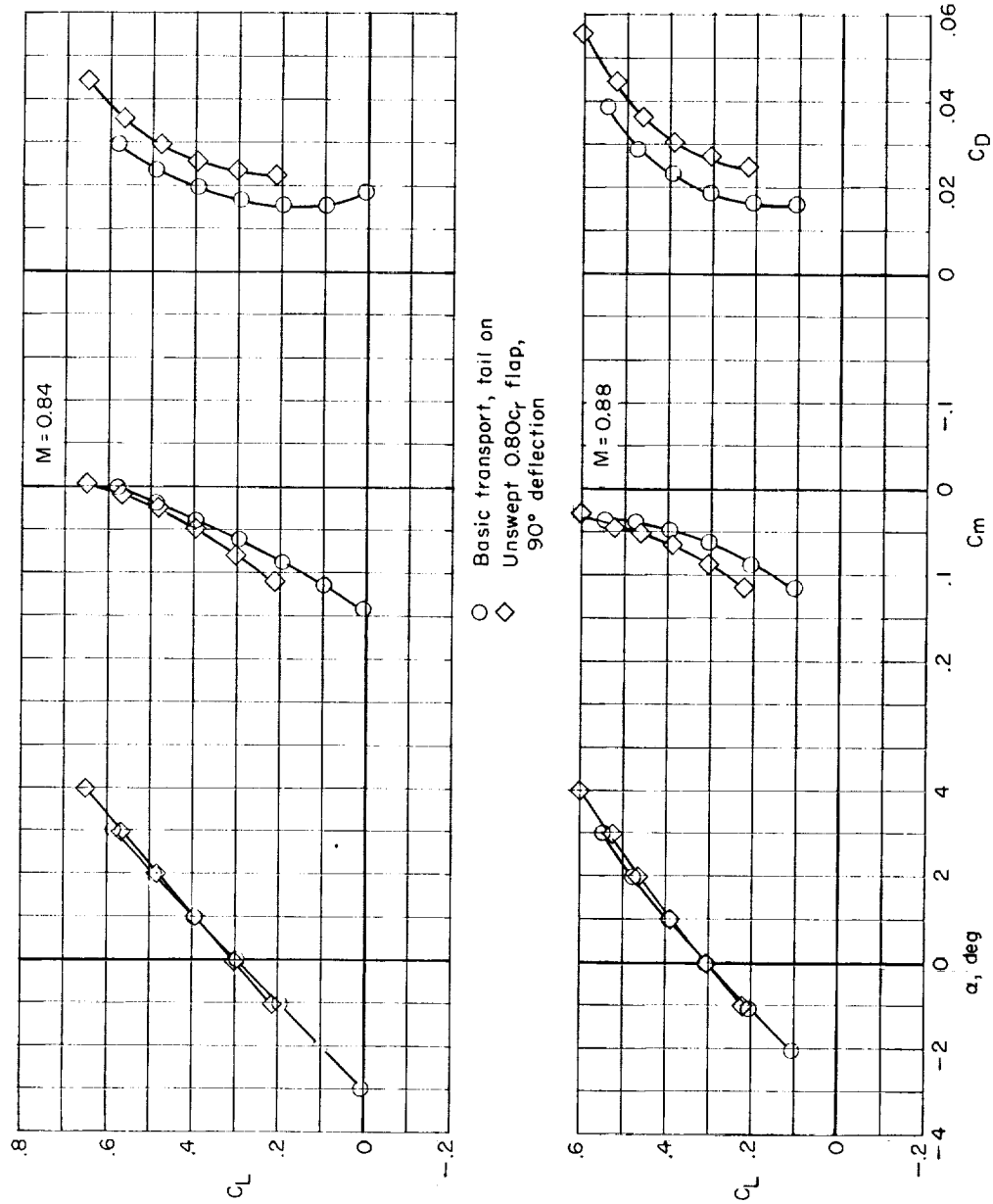

(b) M = 0.84 and 0.88.

Figure 10.- Continued.

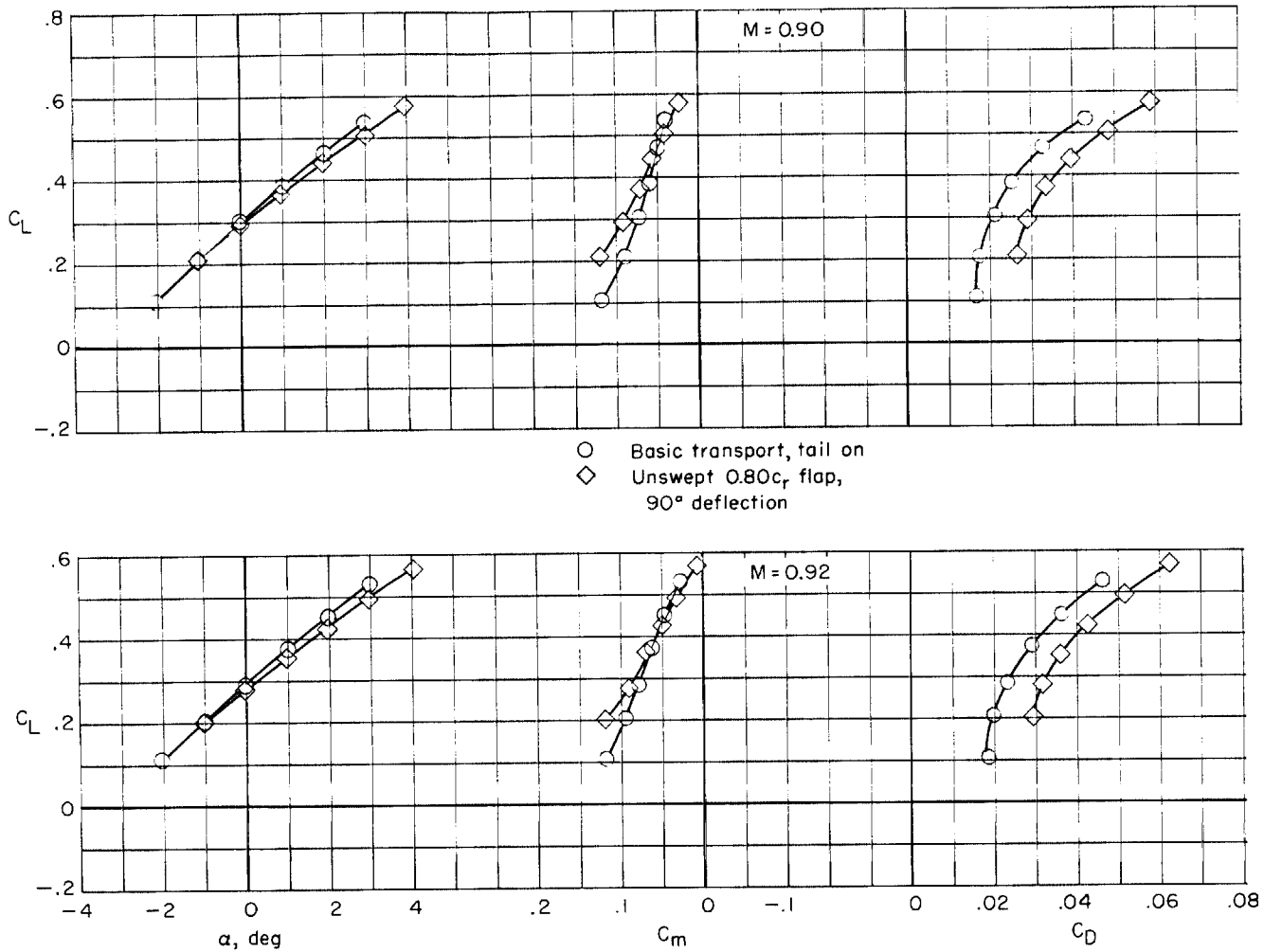

(c) M = 0.90 and 0.92.

Figure 10.- Concluded.

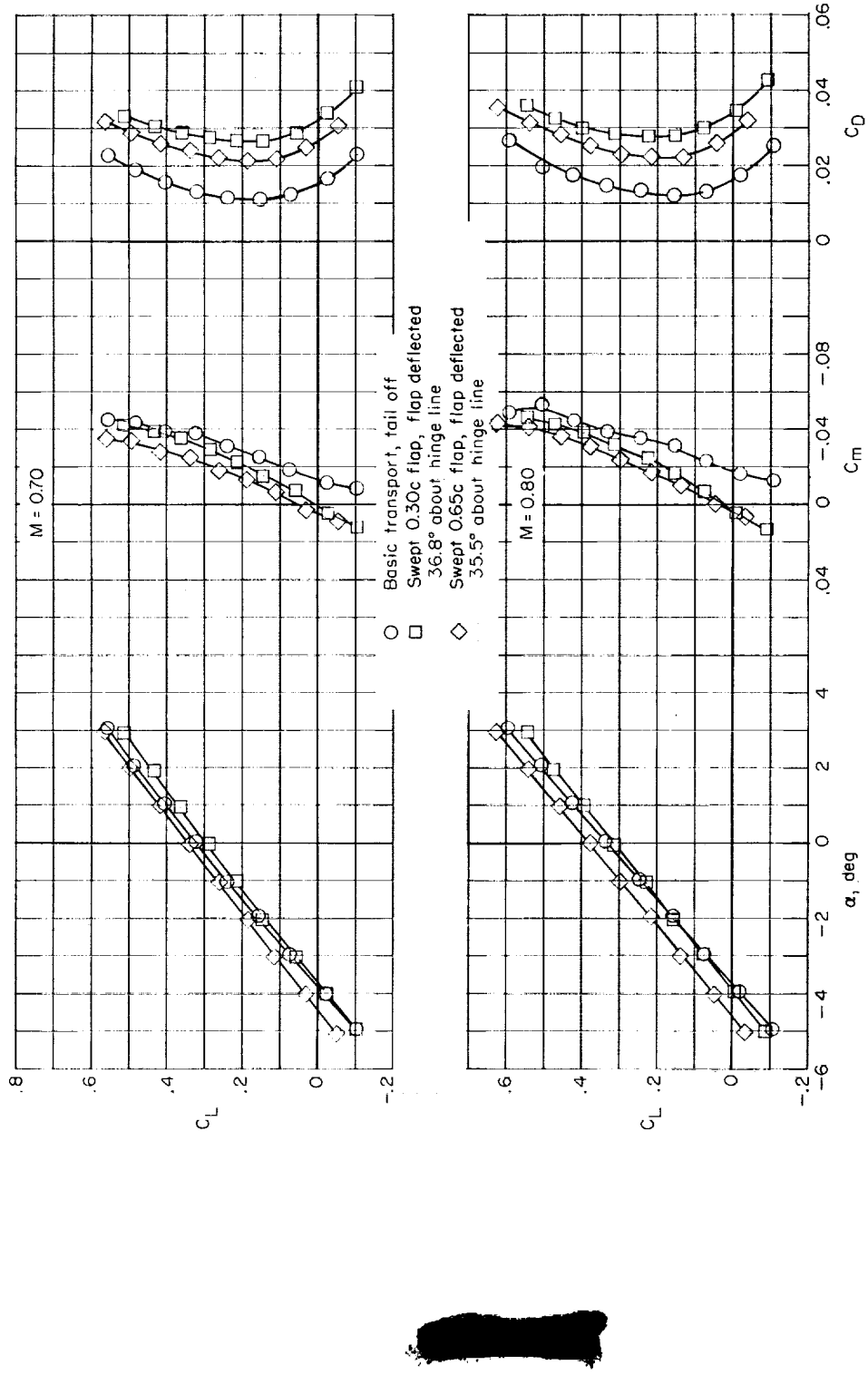

(a) M = 0.70 and 0.80.

Figure 11.- Effect of swept-flap locations on longitudinal stability characteristics of transport model. Horizontal tail off.

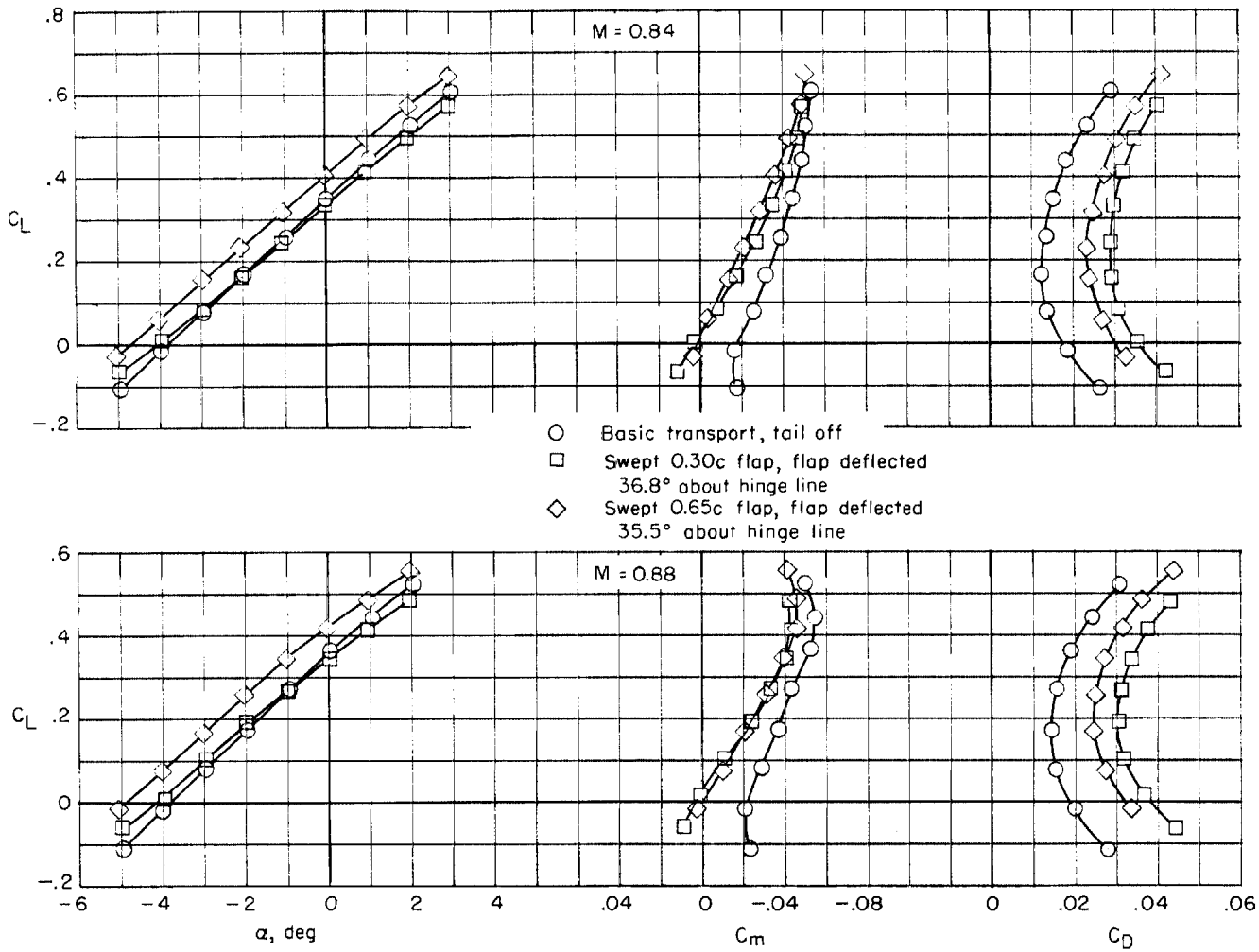

(b) M = 0.84 and 0.88.

Figure 11.- Continued.

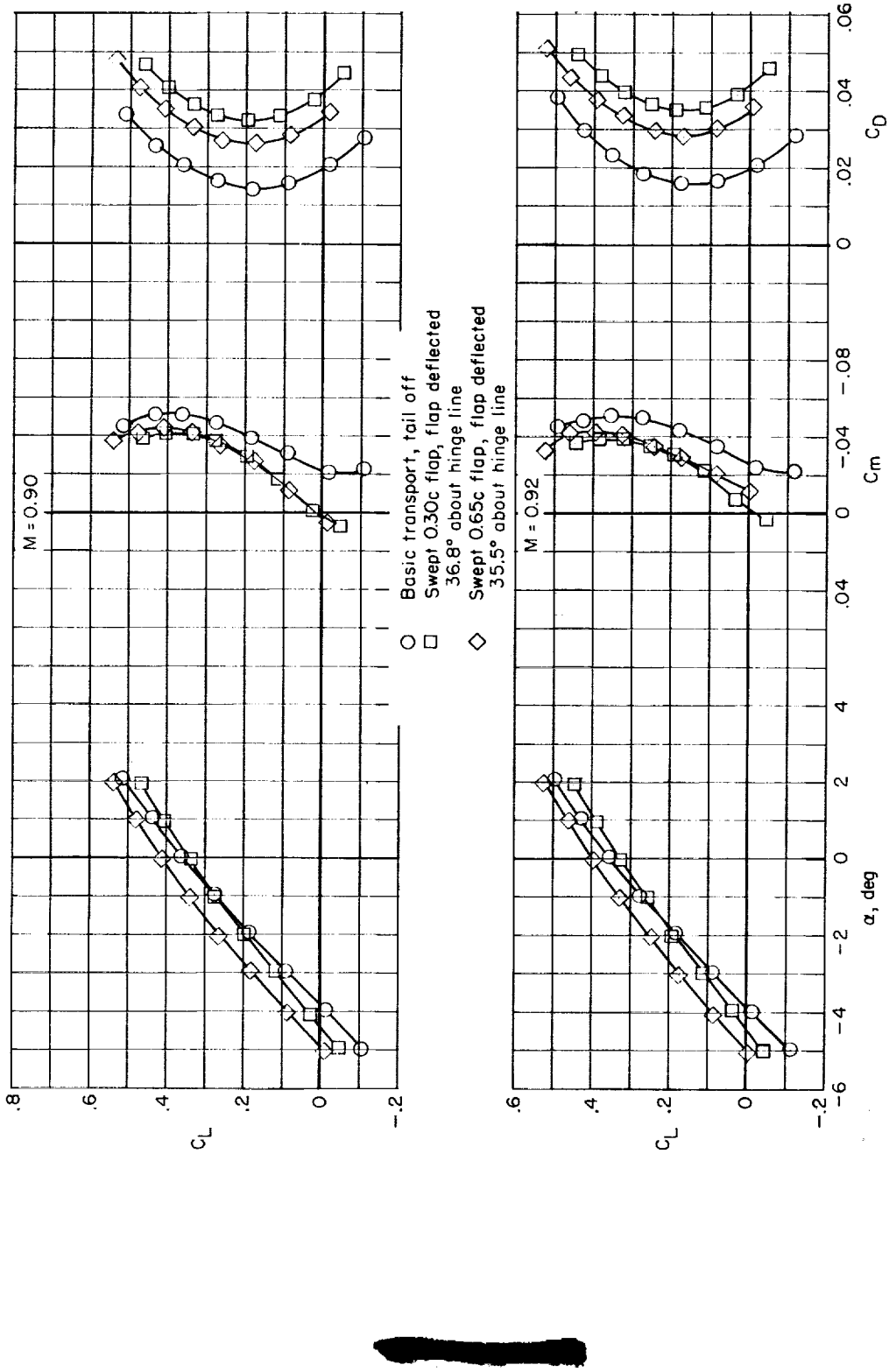

(c) M = 0.90 and 0.92.

Figure 11.- Concluded.

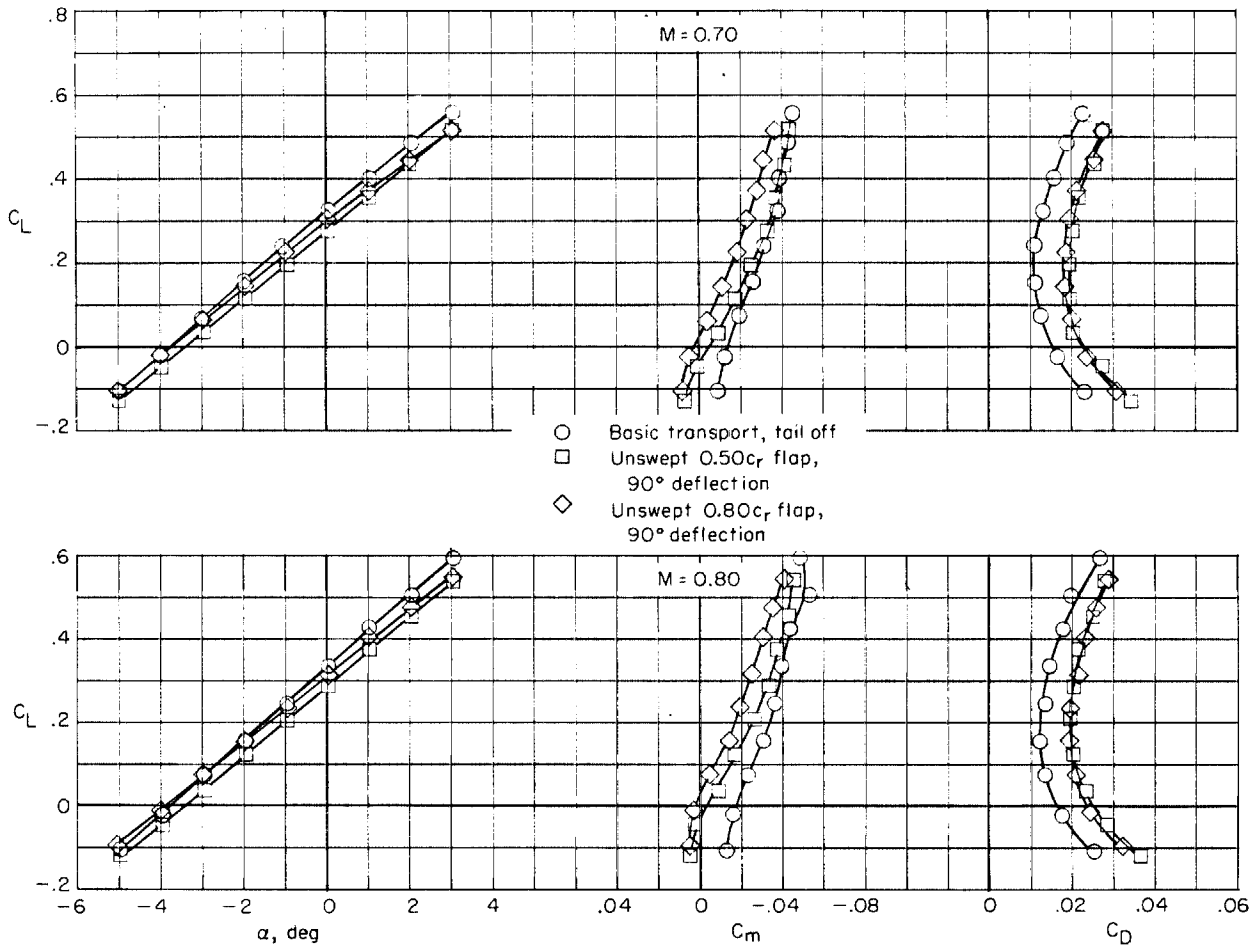

(a) M = 0.70 and 0.80.

Figure 12.- Effect of unswept-flap locations on longitudinal stability characteristics of transport model. Horizontal tail off.

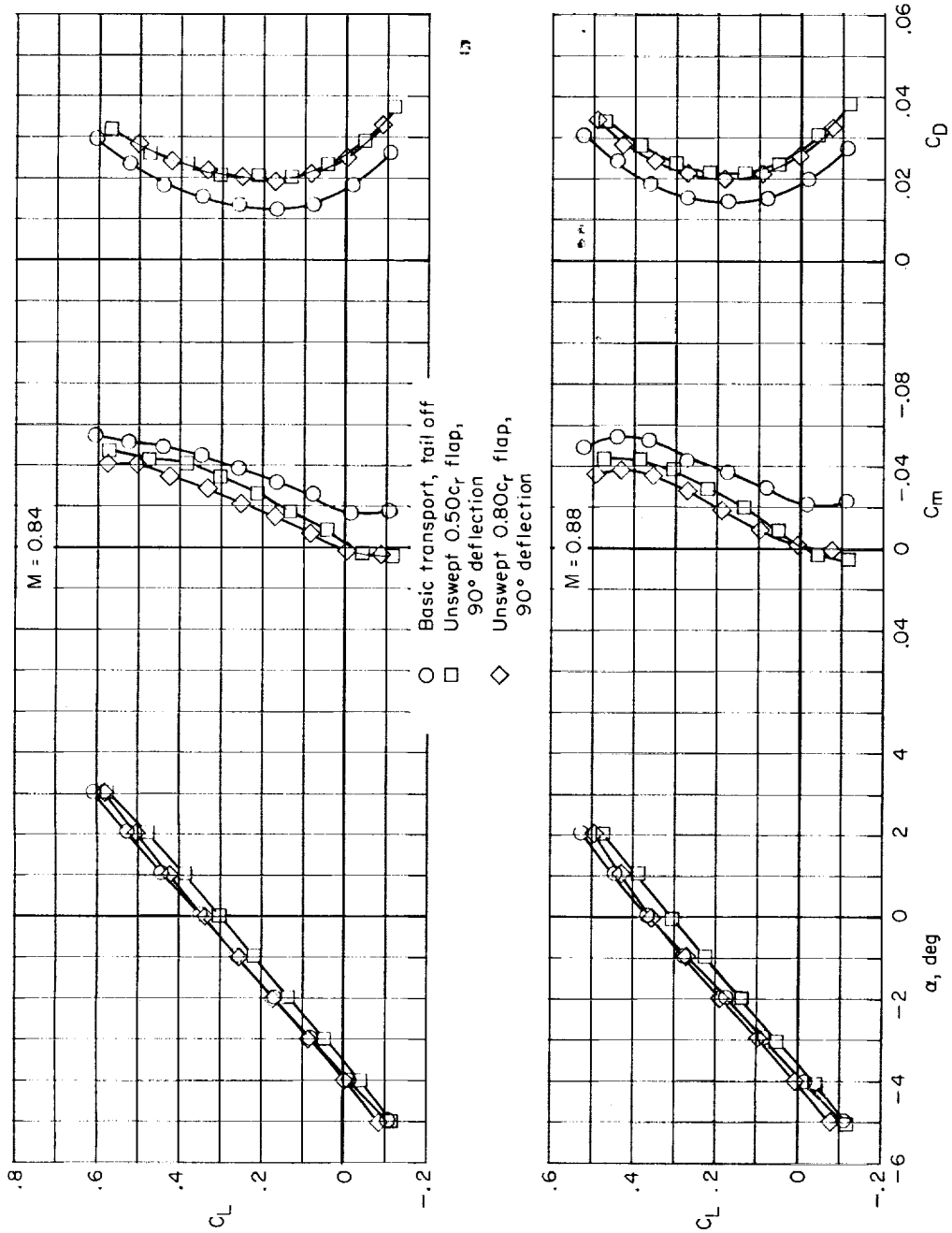

(b) M = 0.84 and 0.88.

Figure 12.- Continued.

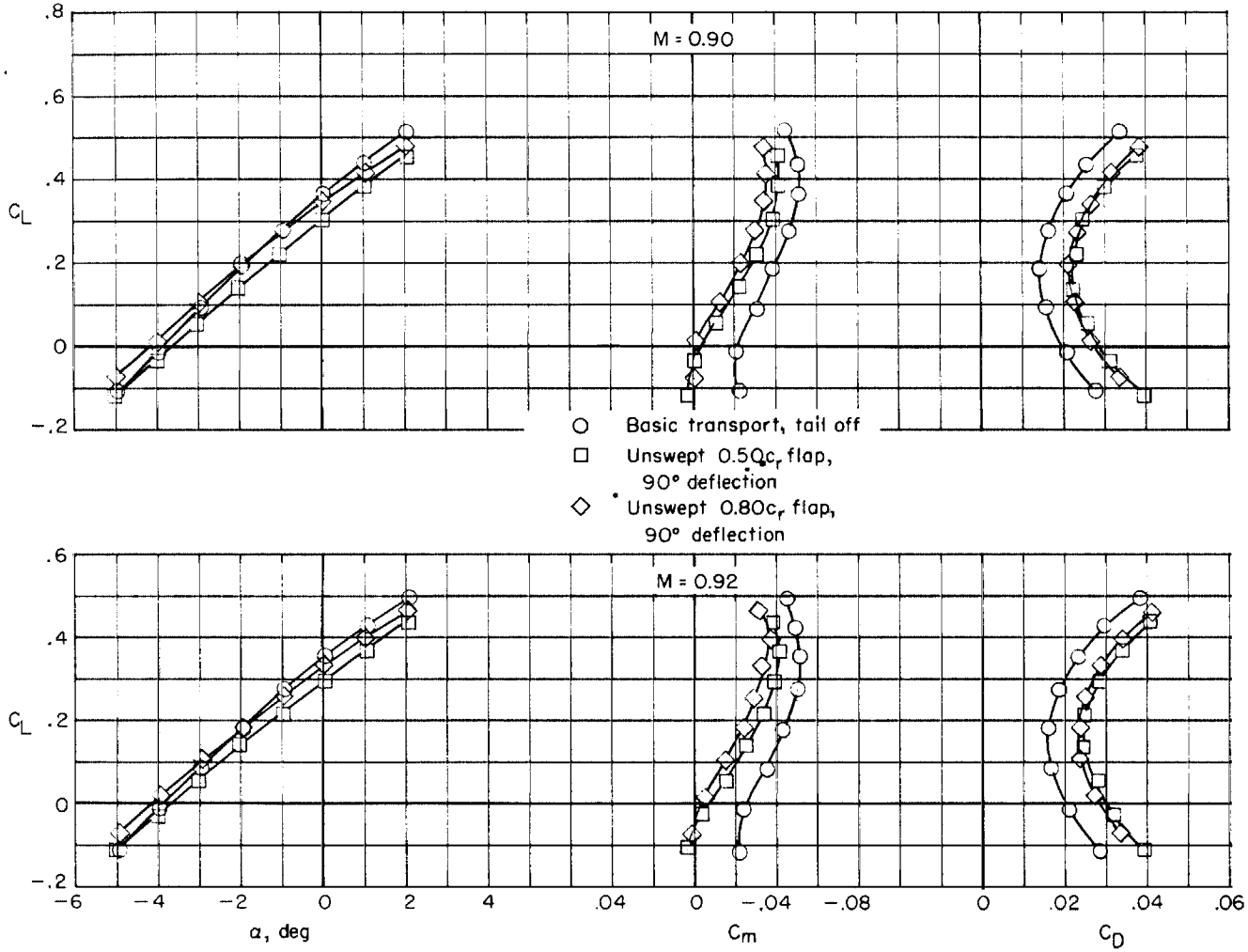

(c) M = 0.90 and 0.92.

Figure 12.- Concluded.

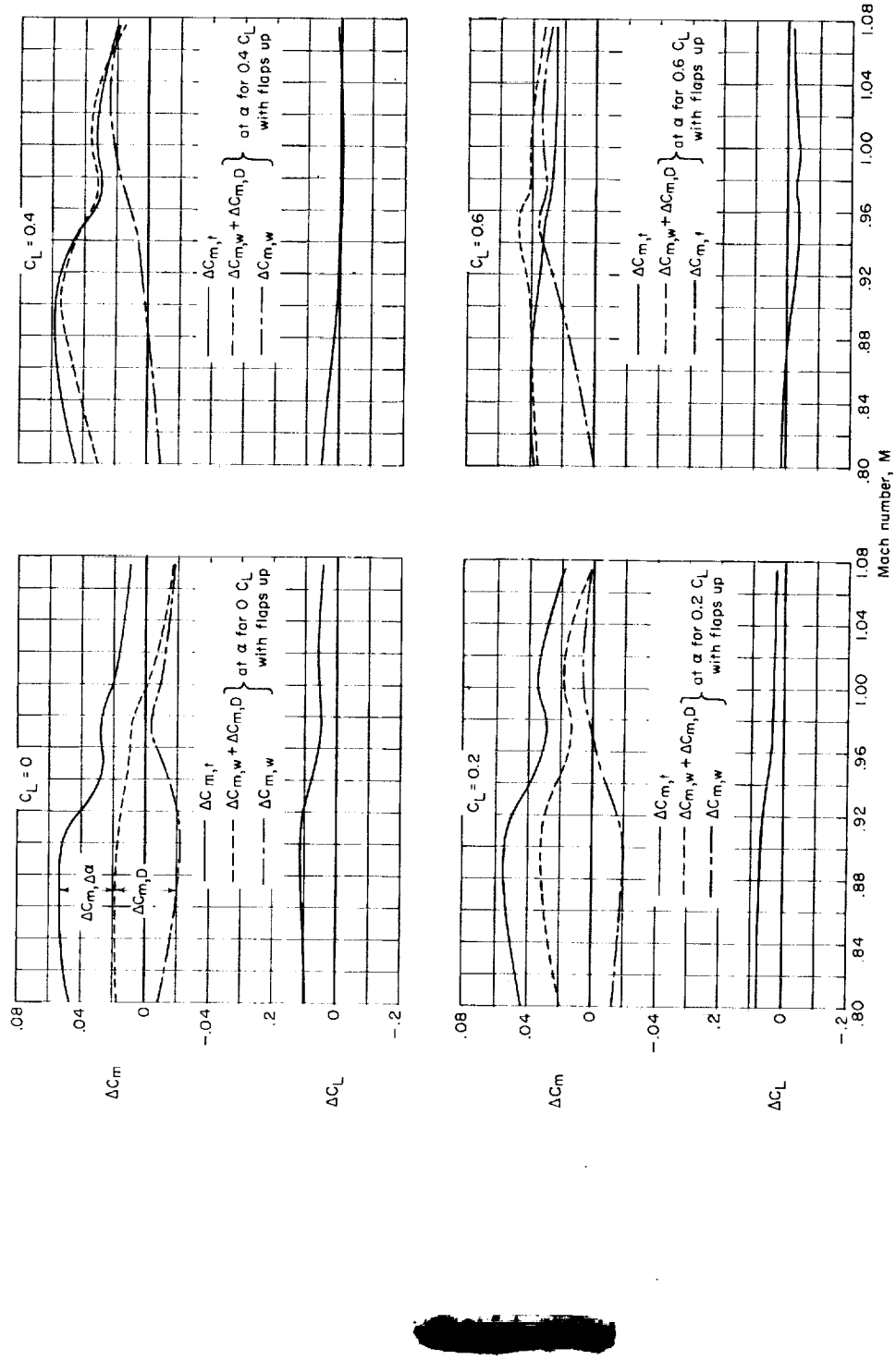

(a) Swept flap; 30° deflection.

Figure 13.- Effect of Mach number on flap effectiveness at various lift coefficients for swept and unswept flaps on seaplane model for various flap deflections.

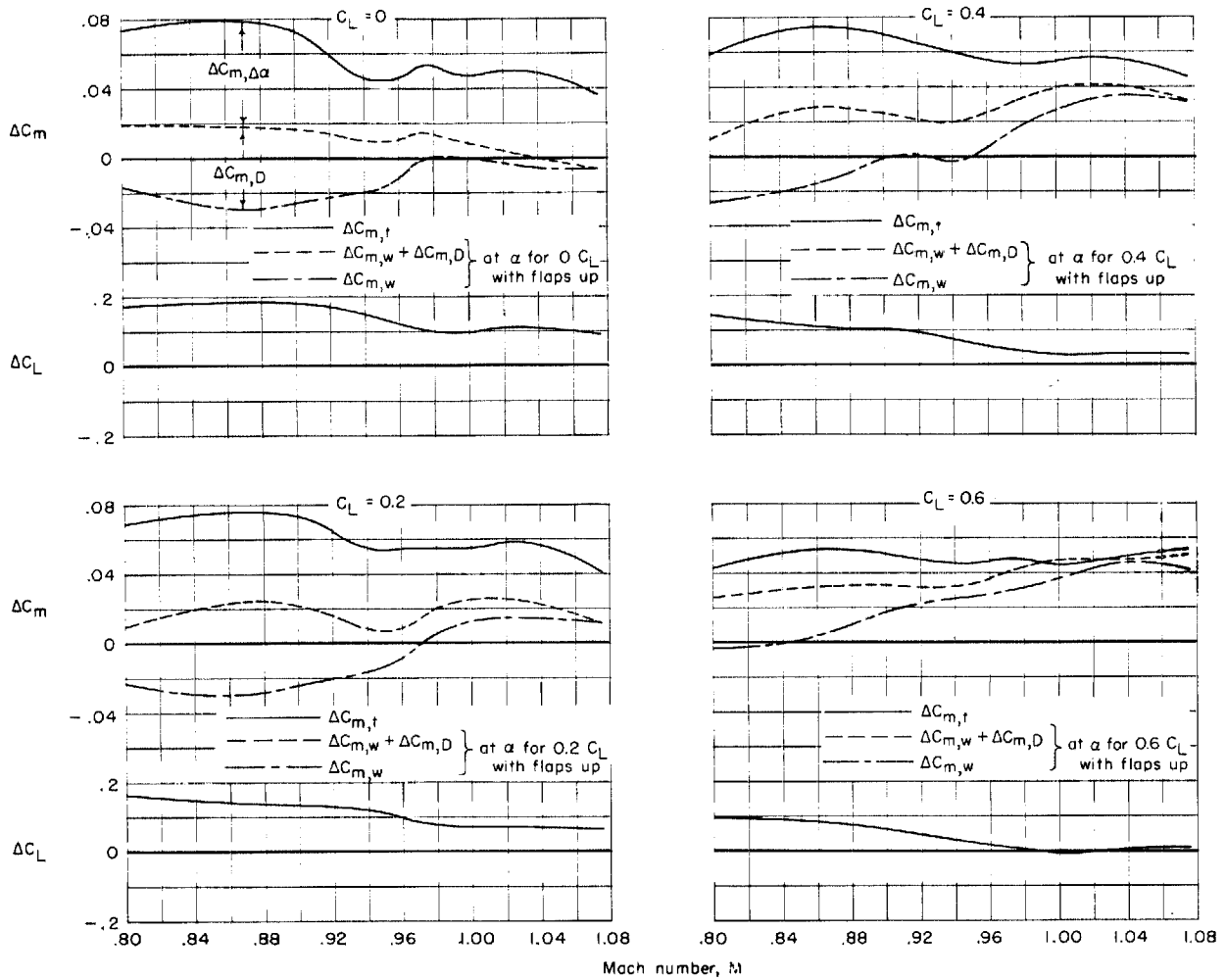

(b) Swept flap; 45° deflection.

Figure 13.- Continued.

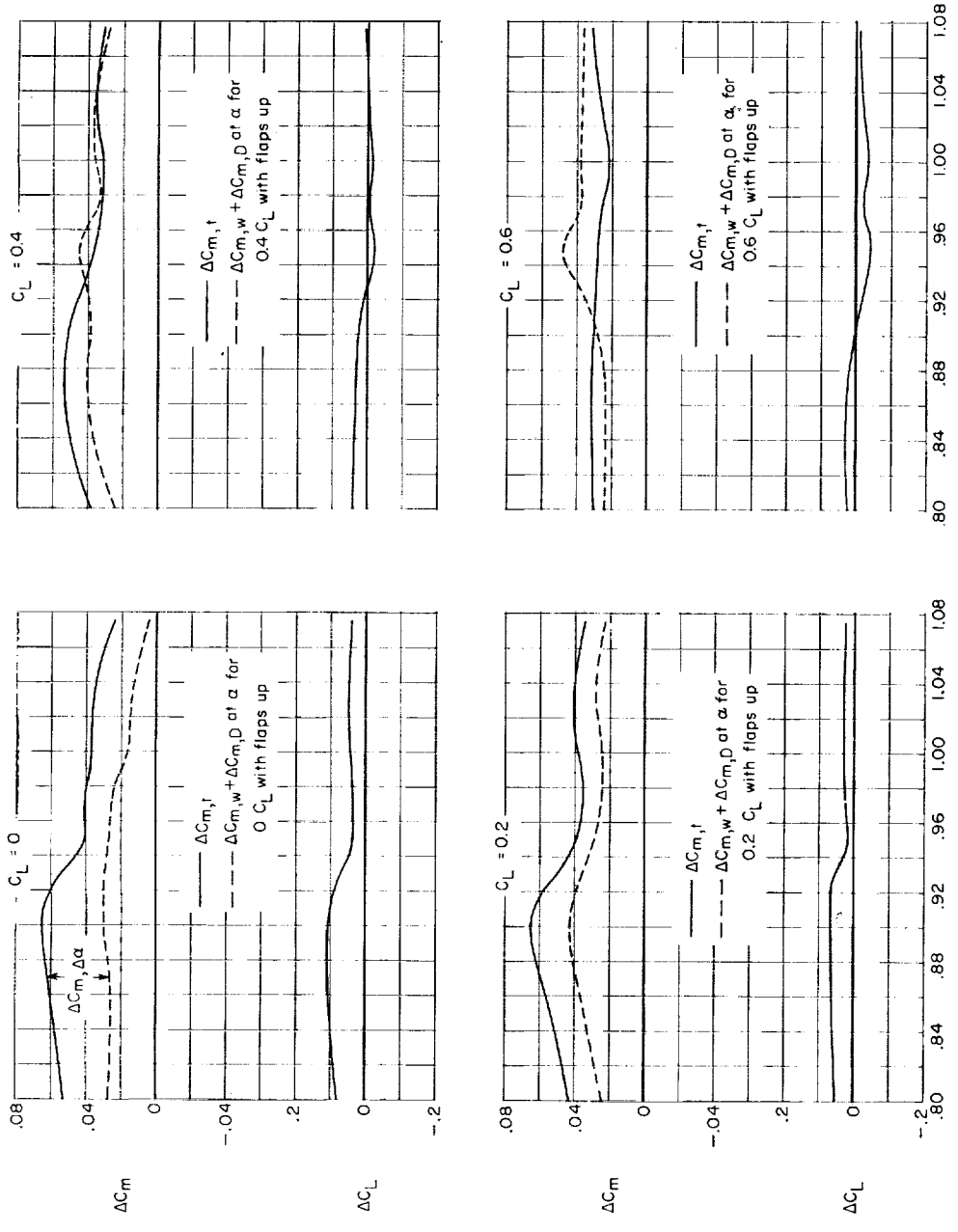

(c) Unswept flap; 30° deflection.

Figure 13.- Concluded.

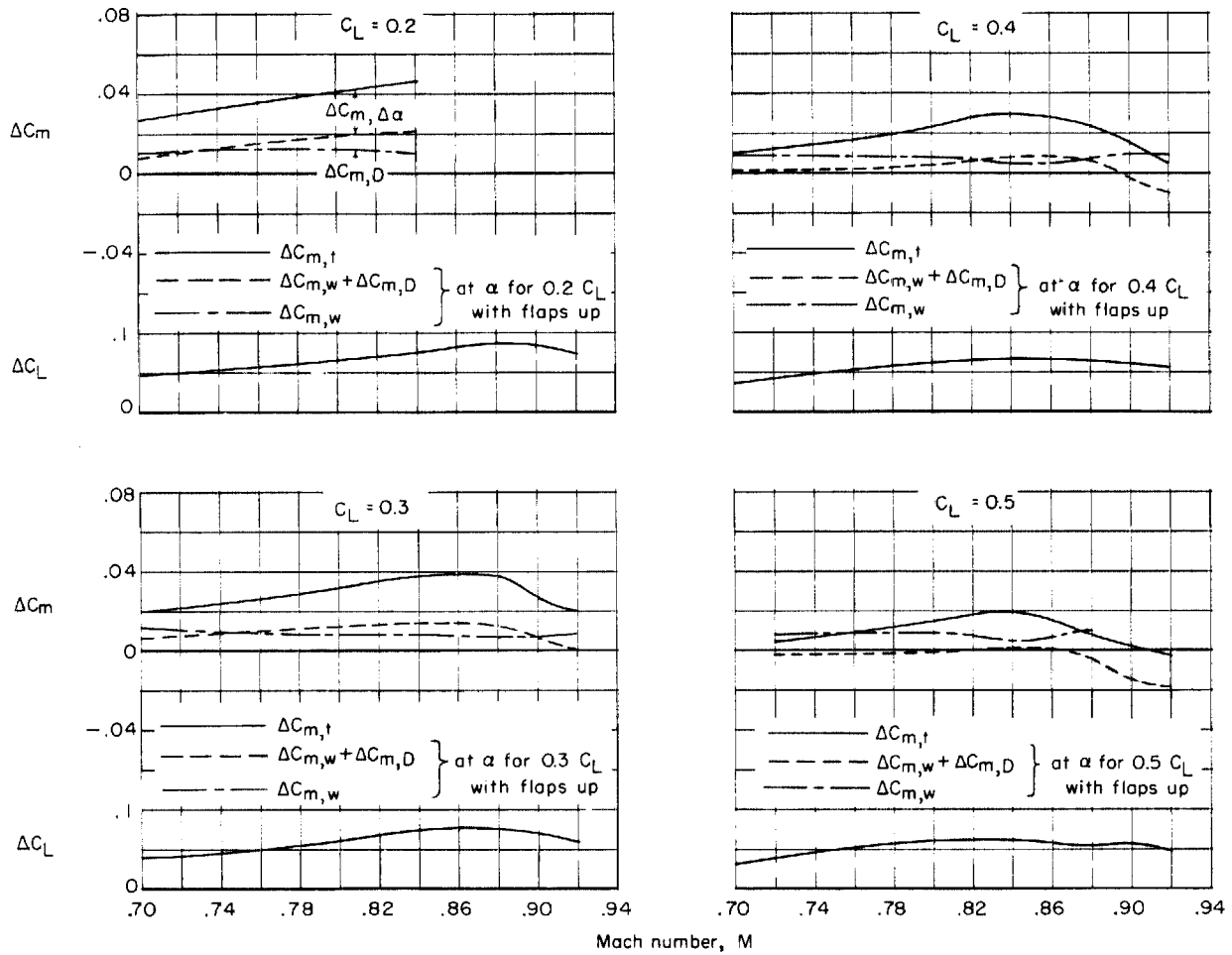

(a) Swept 0.65c flap; flap deflected 35.5° about hinge line.

Figure 14.- Effect of Mach number on flap effectiveness at various lift coefficients for swept and unswept flaps on transport model.

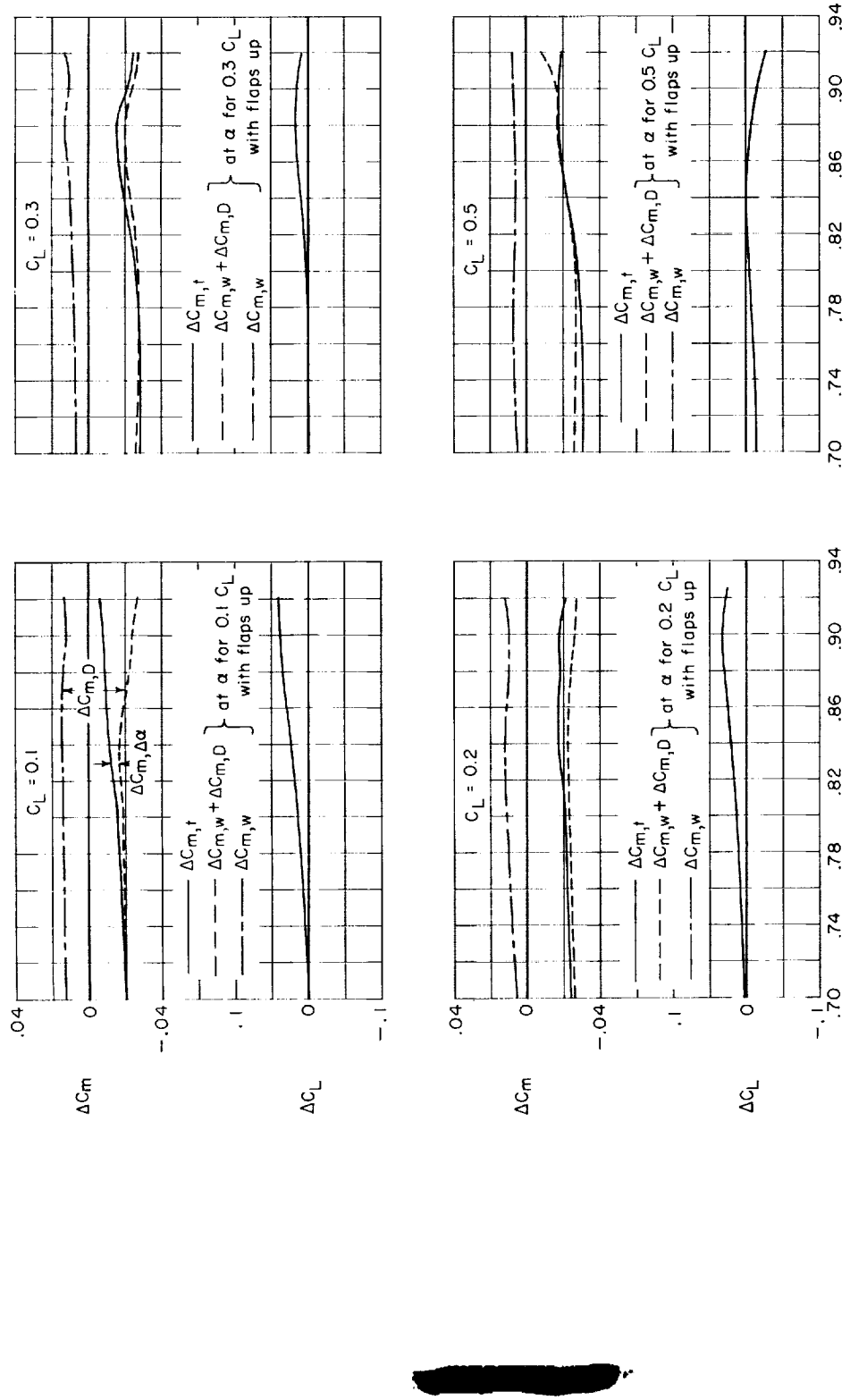

(b) Swept 0.30c flap; flap deflected 36.8° about hinge line.

Figure 14.- Continued.

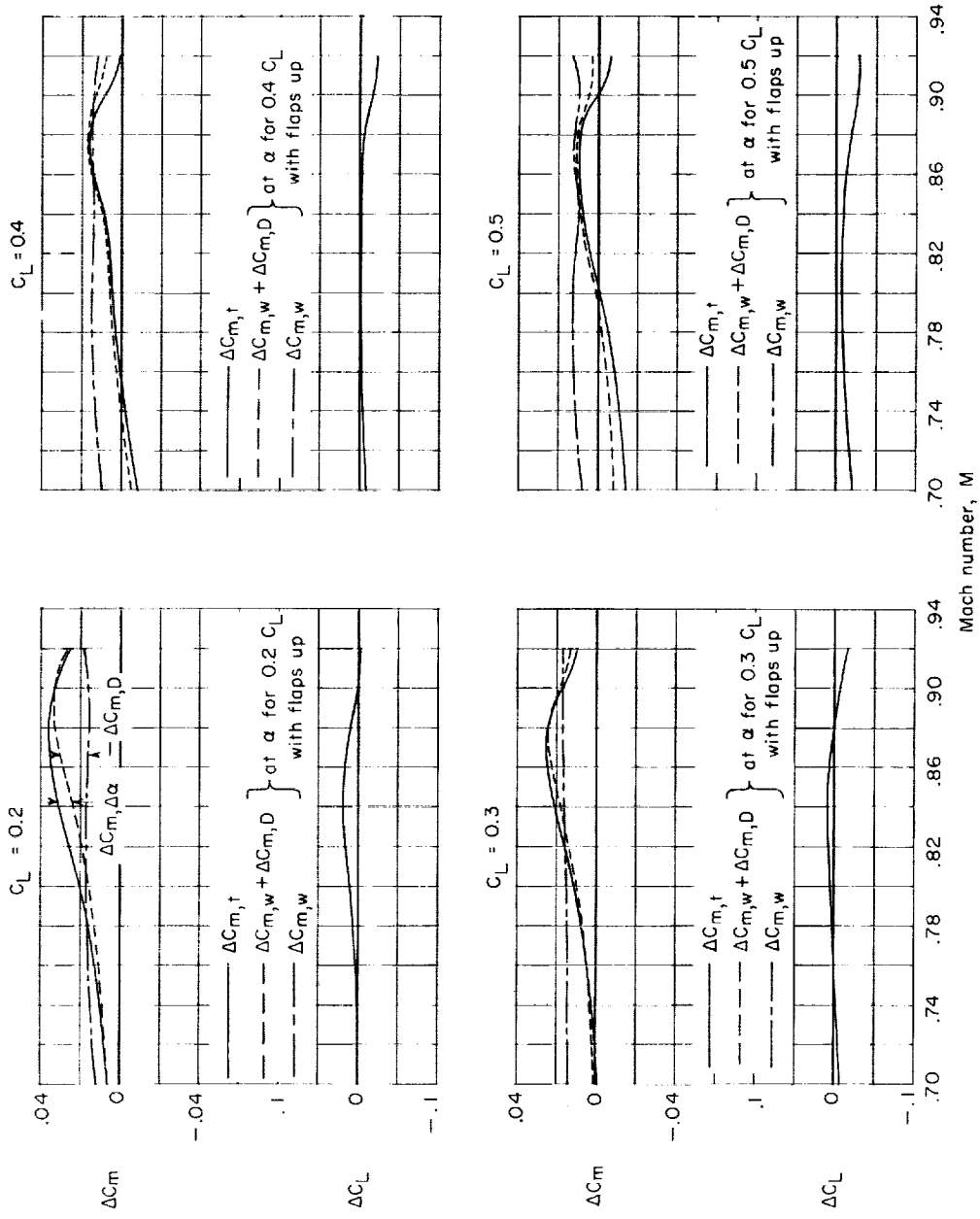

(c) Unswept 0.80c_r flap; 90° deflection.

Figure 14.- Concluded.

NASA - Langley Field, Va. L-292